IMPACT OF COLD-DEACCLIMATION ON BROWN ADIPOSE TISSUE MITOCHONDRIAL ENERGETICS, STRUCTURE AND MITOPHAGY

Nidhi Kuksal

Thesis submitted to the University of Ottawa
in partial fulfillment of the requirements for the
Master of Science in Biochemistry

Department of Biochemistry, Microbiology and Immunology
Faculty of Medicine
University of Ottawa

Abstract

Brown adipose tissue (BAT) generates heat through non-shivering thermogenesis (NST) to help animals adapt to cold environments. Adaptation to cold induces several molecular processes in BAT, including increased uncoupling protein 1 (UCP1) expression, mitochondrial number, and mitochondrial activity. However, the mechanisms governing the deactivation of NST during cold-deacclimation in BAT remain unclear. Our study examines the changes in mitochondrial content, structure, and energetics in C57BL6/J (WT) mice and mito-QC reporter mice at several time intervals (3 hours, 12 hours, 24 hours, and 48 hours) after moving from a cold-adapted state (7 days at 4°C) to a thermoneutral environment (30°C).

We hypothesized that during cold-deacclimation BAT mitochondrial content decreases, mitophagy increases, cristae structure changes, cristae surface area decreases, and oxidative activity decreases. Investigations included mito-QC mice, which express fusion protein (mCherry-GFP) in the mitochondrial outer membrane; during mitophagy the GFP fluorescence diminishes while mCherry fluorescence is preserved. Findings revealed an increase in mitophagy in BAT at 48 hours of cold-deacclimation ($p=0.05$). However, no changes were observed in key autophagy and apoptotic proteins Parkin, LC3I/II or Beclin in BAT during cold-deacclimation. Fission and fusion markers FIS1 and OPA1 remained unchanged, but FUNDC1 and MFN1 decreased at 48 hours, suggesting mitochondrial fragmentation ($p<0.05$). Quantitative analysis of transmission electron micrographs demonstrated a decrease in mitochondrial/cytoplasmic area by 48 hours ($p<0.001$), indicating reduced mitochondrial content. Lipid droplet/cytoplasmic area increased by approximately 50% at 48 hours ($p<0.01$), consistent with reduced lipolysis during adaptation to thermoneutrality.

High-resolution respirometry of permeabilized BAT explants revealed decreased complex I-supported uncoupling at 24 hours ($p<0.001$) and 48 hours ($p<0.01$). Complex II-mediated uncoupled respiration decreased at 48 hours ($p<0.05$), while complex III-derived uncoupled respiration decreased at 3 hours ($p<0.05$), 24 hours ($p<0.05$), and 48 hours ($p<0.001$). Isolated BAT mitochondria exhibited reduced Complex II ($p<0.05$) and III-mediated uncoupled respiration ($p<0.01$) at 48 hours. Both total protein content per milligram of tissue ($p=0.0001$) and total mitochondrial protein per milligram of tissue ($p<0.05$) decreased over time. However, total UCP1 protein content in BAT remained unchanged over the 48-hour period.

Findings overall are consistent with the conclusion that cold-deacclimation decreases mitochondrial content and oxidative activity with increased mitophagy in BAT. Future research directions include investigating details of metabolic changes in BAT during cold-deacclimation using metabolomics.

Acknowledgments

I want to thank Dr. Mary Ellen Harper for giving me the opportunity to study under her guidance, for meeting weekly to discuss my progress, her constant motivation and support to complete my graduate studies. I am very grateful to study under such an understanding and empathetic supervisor.

I would also like to thank Dr. Chantal Pileggi for her constant support, guidance, and friendship. I would also like to thank my lab members for their support throughout my graduate studies. Finally, I would like to thank my friends, family, and my loved ones. Their support, encouragement, motivation, and love helped me get through the joys and hardships in life and during this graduate course.

Table of Contents

List of Figures

List of Tables

List of Abbreviations

ATG-autophagy-related protein

BAT-brown adipose tissue

bFGF- basic fibroblast growth factor

BMR-basal metabolic rates

BNIP3- BCL2adeno virus E1B 19 kDa-interacting protein 3

BSA-bovine serum albumin

^{11}C-acetate-PET -^{11}C-Acetate Positron Emission Tomography

cAMP-cyclic adenosine monophosphate

CL-Cardiolipin

CLox-oxidized cardiolipin

CLAMS-Comprehensive lab animal monitoring system

CNS-central nervous system

COX-2-cyclooxygenase-2

DEE-daily energy expenditure

DIO-deiodinases

DIT-diet-induced thermogenesis

DNM1L-dynamin-1-like protein

DRP1- Dynamin 1-like protein

ETC-electron transport chain

ECD-evolutionarily conserved domain

eWAT-epididymal white adipose tissue

FCCP -carbonyl cyanide p-trifluoro-methoxyphenyl hydrazone

^{18}FDG-PET -18F-Fluorodeoxyglucose Positron Emission Tomography

FFA-free fatty acid

^{18}F-FTHA-PET -^{18}F-Fluorothiaheptadecanoic Acid Positron Emission Tomography

FIS1-mitochondrial fission 1 protein

FUNDC1-FUN14 domain-containing protein 1

G3P-glycerol 3-phosphate

GFP-green fluorescent protein

GLUT1-glucose transporter 1

GLUT4-glucose transporter 4

GTP-Guanosine triphosphate

H &E-hematoxylin and eosin

HRR-high-resolution respirometry

iBAT-interscapular BAT

IMM-inner mitochondrial membrane

IRS-insulin receptor substrate

LC3- light chain 3

MDV-mitochondrial derived vesicles

MFN1/2-mitofusin-1/2

MiRO5-mitochondrial respiration medium

MMP-mitochondrial membrane pore

mPTP -mitochondrial permeability transition pore

mtDNA-mitochondrial deoxyribonucleic acid

mTORC1-mammalian target of rapamycin complex 1

mTORC2-mammalian target of rapamycin complex 2

mtTFA-mitochondrial transcription factor A

MUFA- monounsaturated fatty acyls

nDNA -nuclear de-oxy ribonucleic acid

NDP52-nuclear dot protein52 kDa

NE-norepinephrine NIX -BNIP3-like

NST-non-shivering thermogenesis

OMM-outer mitochondrial membrane

OPTN-optineurin

OXPHOS-oxidative phosphorylation

p38MAPK -p38 mitogen-activated protein kinases

p-car -palmitoyl-carnitine

PAI1-plasminogen activator inhibitor 1

PE-phosphatidylethanolamine

PEDF-pigment epithelium derived factor

PET-positron emission tomography

PGAM-phosphoglycerate mutase

PGC1-α-peroxisome proliferator-activated receptor (PPAR)-γ coactivator

PI3K-phosphatidylinositol 3-kinase

PINK1-PTEN-induced kinase 1

PPARγ-peroxisome proliferator-activated receptor

PPP-pentose phosphate pathway

PRCF-percentage relative cumulative frequency

PRKAA-protein kinase AMP-activated

PUFA- polyunsaturated fatty acyls

PVDF-polyvinylidene fluoride

RER-respiratory exchange ratio

RIPA-radio-Immunoprecipitation assay buffer

ROS-reactive oxygen species

RWAT-Retroperitoneal white adipose tissue

sBAT-subscapular BAT

SFA-saturated fatty acids

SNS-sympathetic nervous system

STK-serine/threonine-kinase

T3-3, 3', 5-triiodothyronine

T4-thyroxine

TAG-triacylglycerol

TAX1BP1-Tax1-binding protein 1

TCA-tricarboxylic acid

TEM-transmission electron microscopy

TREs-thyroid response elements of genes

UCP1-uncoupling protein 1

ULK1/2-Unc-51-like autophagy activating kinase ½

VCO2-volume of carbon-di-oxide production

VDAC -voltage-dependent anion-selective channel

VEGF-vascular endothelial growth factor

VEGF-A-vascular endothelial growth factor-A

VEGF-B-vascular endothelial growth factor-B

VEGFR2-Vascular endothelial growth factor receptor 2

VEGF 120-vascular endothelial growth factor 120

VO2-volume of oxygen consumption

WAT- white adipose tissue

β3ARs- β3-adrenergic receptor

1. Introduction

1.1 Adipose tissue

Adipose tissue can be categorized into three general types based on morphology and physiological functions. These types include white adipose tissue, brown adipose tissue, and beige adipose tissue. White adipose tissue (WAT) is an endocrine organ essential in maintaining metabolic homeostasis by storing energy derived from food[1–3]. Brown adipose tissue (BAT) has unique structural characteristics and is highly thermogenic through a process referred to as non-shivering thermogenesis (NST)[4,5]. Whereas beige adipose tissue can generally be described as having intermediate phenotypic characteristics between WAT and BAT. Thus, these distinct types of adipose tissue play critical roles in mammalian physiology.

1.1.1 White adipose tissue

White adipose tissue (WAT) is broadly classified as subcutaneous (under the skin), which constitutes about 80-85% of body fat, and visceral fat (intra-abdominal), which constitutes about 10-20% of body fat in adult humans[6–9]. Both these types of WAT differ in their properties and functions[6, 10]**.** The primary function of WAT is to take up glucose and fatty acids, and to store the energy as triglycerides; this results in a unilocular lipid droplet [11]. Increased energy intake expands adipose tissue to store surplus lipids[12, 13]. Although WAT contributes to a small fraction of total energy expenditure (5- 10%), it is vital for balancing fat levels in the body[14, 15].

Conversely, stored triglycerides are catabolized into free fatty acid during periods of increased energy expenditure, exercise, cold adaptation or fasting[16]. Additionally, a vast array of growth factors, enzymes, cytokines, hormones, and proteins are secreted by WAT to maintain overall health[17–21]. All these biological regulators work together to support numerous physiological processes. Moreover, apart from lipid metabolism, WAT has multifaceted roles in reproduction, angiogenesis, immunity, coagulation, and fibrinolysis[18, 22–24].

1.2 Brown adipose tissue

Brown adipose tissue is an “energy-burning tissue,” constituting less than 0.5% of body weight in adult humans, and is highly vascularised with abundant mitochondria and small lipid droplets[25–30]. Active BAT has been estimated to elevate basal energy expenditure by 1-7% in male adults[29, 31–

[33], but this remains controversial. In humans, BAT is found in the peri-renal, cervical, supraclavicular, axillary, paravertebral, peri-aortic, and interscapular regions[27, 29, 32, 34–38]. The distribution of BAT changes in humans with age. In infants, BAT is predominately found in the interscapular and perirenal regions[34, 35, 39–41]. In adults, BAT is predominately found in the cervical, supraclavicular, and paravertebral regions, with the supraclavicular depot being the most commonly studied depot[34, 35, 39–41]. In rats, 50–60 % of BAT was found in intrascapular and cervical regions and 25 % of BAT was found around the kidneys[42–44].

An inverse co-relation was found between BAT activity and body-mass index (BMI) in human adults undergoing PET/CT scans[27, 45, 46]. BAT is also present in many other mammals, but its anatomical location might vary depending on the type of species[39, 47–49]. While the size and composition can vary between mouse strains and sex, iBAT is the largest depot[37, 50]. Understanding the intricacies of BAT distribution would help to understand its role in whole-body metabolism.

1.2.1 Uncoupling protein 1 (UCP1)

The key feature of BAT is its ability to produce heat through NST, a process that relies on mitochondrial uncoupling[51]. The mitochondrial electron transport chain (ETC) is composed of complexes I-IV through which electrons pass while pumping protons from the matrix into the mitochondrial intermembrane space[52]. In coupled thermogenic processes, protons return to the matrix through CV (ATP synthase). However, under uncoupled thermogenic states protons return into the matrix bypassing ATP synthase[53].

Uncoupling protein 1 (UCP1) also known as "thermogenin'', is a ~32kDa protein located in the mitochondrial inner membrane and represents about 10% of total mitochondrial protein in BAT [51, 54–57]. UCP1 is exclusively expressed in BAT; other UCPs are expressed also in BAT and elsewhere in the body[58, 59]. Like other proteins in the SLC25 family, UCP1 has six transmembrane α-helices that are connected by extra-membrane loops[48, 60]. Usually, UCP1 remains in its inactivated cytosolic state (c-state) where purine nucleotides such as guanosine triphosphate (GTP) bind to inhibit proton leak[61]. UCP1 is activated by cold environmental temperatures through the sympathetic nervous system (SNS); its thermogenic capacity is augmented by thyroid hormones and activity can be modulated through changes in cellular

redox and reactive oxygen species (ROS), etc[62–64]. Purine nucleotides, such as guanosine diphosphate (GDP) and ADP, inhibit UCP1, whereas fatty acids activate it [65–67]. Specifically, a competitive model has been proposed where fatty acids compete with GDP to control UCP1 mediated leak[68–72]. Fatty acids also increase the mRNA expression of UCP1 and related genes through PPRE promoter sequences, increasing thermogenesis supported by increased glucose and fatty acid oxidation[61, 73–78].

Upon activation, UCP1 facilitates proton (H+) leak from the mitochondrial intermembrane space into the mitochondrial matrix. UCP1 transitions to its matrix (m-state) to cause proton leak, which in turns stimulates upstream fuel oxidation pathways, and this 'work' is what generates the heat [61, 79, 80]. Taken together, UCP1 is the key controller of thermogenesis for whole body thermoregulation[81]. Apart from UCP1, uncoupling protein 3 (UCP3) present in the mitochondrial inner membrane of BAT mitochondria is homologous to UCP1 by ~70%[82–84]. Although UCP3 levels are estimated to be roughly 400-fold lower than UCP1, it has been shown to limit oxidative damage in BAT[85, 86]. Thus, this highly metabolic tissue BAT has garnered significant attention in the field of metabolic biochemistry.

1.2.2 Beige adipose tissue

Beige adipose tissue, also known as "brite" adipose tissue, was found to have a metabolic rate higher than WAT and lower than BAT[87]. In terms of functions, beige adipose tissue participates in storing energy as well as NST[88]. Interestingly, some white adipocytes can convert into beige adipocytes under the influence of certain stimuli (cold, or treatment with adrenergic agonists) through a process called browning. During this process beige adipocytes are recruited in WAT to increase mitochondrial number and to upregulate the expression of thermogenic genes[89]. Browning increases the amount and the activity of UCP1 allowing the cells to attain brown adipocyte-like appearances and functions.

Upon stimulation, WAT begins to express low levels of thermogenic genes, such as UCP1, to initiate browning[90–92]. Browning of specific WAT depots in mice is influenced by sex, where the inguinal depot browns better in males while peri-ovarian depot browns efficiently in females[89, 93–95]. Cold exposure is a profound stimulus to induce browning. A study in rodents showed a ~7-fold increase in the mRNA expression of UCP in periovarian WAT upon cold

exposure (4°C) for 10 days[96]. Moreover, β-adrenergic agonist (BRL 26830A, 10 mg/kg i.p.) or CL316, 243 were shown to increase UCP1 expression in WAT to induce browning in rats and mice[96, 97]. Another study, where Zucker rats were treated with the β-adrenergic agonist, CL 316,243 (1mg/kg/d) for 2-3 weeks, also showed recruitment of brown adipocytes within retroperitoneal white adipose tissue (RWAT) and epididymal white adipose tissue (eWAT) [98]. The treatment with capsinoids, green tea, fish oil, and curcumin was also found to contribute to beiging/browning[99, 100].

Browning of WAT enhances energy expenditure and improves glucose and lipid metabolism[101, 102]. Although the significance of beige adipocytes is not clearly understood, the role of beige adipose tissue in several metabolic disorders like obesity and diabetes is of ongoing interest.

1.3 Effect of cold-acclimation in BAT

Cold exposure induces a cascade of biochemical and physiological changes in BAT, causing morphological and functional changes in BAT. An in-depth understanding of the effects of environmental cold on BAT can provide insights into metabolism and help identify potential strategies for managing metabolic disorders. The following sections review process of adrenergic activation, as well as morphological, and functional changes that occur in BAT during cold exposure and acclimation.

1.3.1 Sympathetic nervous system

The hypothalamic areas of the brain are responsible for controlling body thermoregulation[103–105]**.** The physiological responses triggered by cold exposure include vasoconstriction, skeletal muscle shivering, and BAT thermogenesis[105, 106]. Cold activation activates the sympathetic nervous system (SNS) dependent β3-adrenergic receptors (β3ARs) to drive BAT activation and thermogenesis with neurochemical signalling[107–110]**.**

Sustained cold exposure stimulates the release of norepinephrine (NE), that bind to β2 and β3 adrenergic receptors to stimulate cAMP-dependent signalling to activate protein kinase A (PKA)[111–113]. The downstream targets of PKA increase lipolysis where triglycerides (TG) release free fatty acids by adipose triglyceride lipase (ATGL) and hormone-sensitive lipase (HSL) [16, 56, 114–117]. PKA activates p38 mitogen-activated protein kinase (p38MAPK) which is necessary for

expression of peroxisome proliferator-activated receptor-γ coactivator (PGC1-α) to stimulate UCP1 expression and mitochondrial biogenesis[118–120]. The promoter regions of UCP1 gene contain canonical peroxisome proliferator-activated receptor (PPAR)-responsive elements (PPREs) and two putative cAMP-responsive elements (CREs) for enhancing UCP1 activity[118, 121]. NE dependent stimulation was found to regulate CRE2 but was not essential for CRE3 mediated UCP1 gene transcription[122]. Interestingly, CRE-binding protein (CREB) was found to bind to CRE to augment the role of the enhancer[123]. Thus, the cAMP pathway is important in transmitting the signals from NE and its downstream effects are vital for controlling heat production and mitochondrial balance in BAT.

1.3.2 Changes in BAT morphology upon cold exposure and acclimation

Cold increases the number of pre-adipocytes that subsequently differentiate into brown adipocytes[110, 111]. The size/ weight of BAT often increases during cold adaptation (10°C and 21°C for 4 weeks) [124]. Haematoxylin and eosin (H &E) staining of iBAT sections revealed depletion of lipid content during cold exposure (4°C for 4h)[125]. Additionally, BAT mitochondria undergo remodelling in response to cold. According to Giordano *et al.*, mitochondria were elongated, and the number of glycogen granules increases when rats were cold acclimated for 2 weeks [126]. Moreover, UCP1 expression, and the total amount of mitochondrial proteins increase in the brown adipocytes of hamsters exposed cold (4°C for 6 days) [56, 127, 128].

1.3.3 Alterations in BAT mitochondria

Mice exposed to chronic cold (4°C for 4 weeks) leads to the activation of UCP1 in BAT and increases β-oxidation and electron transport chain (ETC) activity[56, 129, 130, 131]. Chronic cold exposure (6°C for 10 days) also elevates the levels of tri-carboxylic acid (TCA) cycle intermediates including citrate, α-ketoglutarate, succinate, fumarate, and malate[132]. Brown adipocytes of mice exposed to cold (4°C for 2-4 days) elevated glucose uptake, pentose phosphate pathway (PPP) flux, glycogen uptake, and glycerol 3-phosphate synthesis [133].

Upregulation of genes encoding mitochondrial ribosomal protein (MrpL3, MrpL15, MrpL20 and MrpL51) and the genes responsible for recycling ribosomal proteins (e.g. Mrrf) was observed in

BAT of mice exposed to cold (8°C ±2°C for 24 h)[134]. However, the same study did not report any changes in the genes involved in BAT differentiation (e.g. Cidea, /PRDM16) or mitochondrial biogenesis (e.g. cytochrome c; cox8b) [134]. However, mitochondrial proteins and cytochrome c oxidase activity were elevated in the BAT of hamsters and mice following 3 weeks of cold-acclimation (6°C) [135].

1.3.3.1 PGC-1 *α* mediated signalling

There are three members of the PGC-1 family (PGC-1α, PGC-1β, and PGC-1-related coactivator). Whole-body PGC1-α and PGC1-β KO mice have impaired expression of mitochondrial genes, reduced oxidative capacity and disrupted thermogenesis[136,137]**.** PGC1-α stimulates mitochondrial biogenesis by coactivating nuclear respiratory factor (NRF) 1 and 2 to increase the expression of mitochondrial transcription factor A (mtTFA)[138]. Additionally, PGC1-α increased the expression of nuclear-encoded genes of the ETC and oxidative phosphorylation (OXPHOS) system[139–141].

Although the expression of PGC1-α is low in liver, it is highly expressed in the brown adipose tissue[142]. In 1998, Puigserver *et al.* discovered PGC1-α in BAT of mice exposed to cold[142]. The 'master regulator' of mitochondrial biogenesis, PGC-1α, plays a key role in BAT thermogenesis. Its levels were elevated by 30-50-fold in BAT of mice exposed to cold (4°C for 3 or 12 h) [142]. Studies have shown PGC1-α to interact with peroxisome proliferator-activated receptor-α (PPARα) to increase UCP1 expression[121, 121, 143]. Apart from inducing UCP1, PGC1-α also interacts with PPARγ to aid brown adipocyte differentiation[144–146]. PGC1-α is essential for thermogenesis as PGC1-α KO mice cannot maintain their body temperature when exposed to cold (4°C for 5h) [136,147].

1.3.3.2 Glucose uptake

Glucose is a vital metabolite in BAT when its mitochondria are uncoupled, and therefore un able to produce ATP through OXPHOS. Studies in rats indicated that cold exposure (4°C for 48h) led to a 95-fold increase in glucose uptake in BAT to support glycolysis for ATP production[148–151]. Upon adrenergic stimulation, apart from fatty acids glucose was also shown to meet the increase in energy demand[152]. In fact, glucose was shown to be utilized by the brown adipocytes during adrenergic stimulation in rats to increase thermogenesis by 16%[153–155].

Glucose transporter 1 (GLUT1) and glucose transporter 4 (GLUT4) are the only glucose

transporters found in BAT[156]. Their expressions are regulated by β3-adrenergic receptor activation of cAMP dependent mechanisms [157,158]. In BAT, GLUT1 facilitates glucose uptake via an insulin-independent mechanism by activating the phosphatidylinositol 3-kinase (PI3K) pathway[159–161]. mRNA expression of GLUT4 increased in rats during cold-acclimation (4°C for 10 days)[162]. Moreover, the KO of GLUT1 and GLUT4 prevented the elevation of oxygen consumption in immortalized brown adipocytes indicating the importance of glucose transporters during thermogenesis[163]. Additionally, GLUT4 inhibitor, indinavir repressed glucose uptake and decreased thermogenesis as measured in mice by infrared thermography[164].

1.3.3.3 Thyroid signalling

Thyroid hormones have a pivotal role in regulating thermogenesis, glucose metabolism, and lipid metabolism in BAT[165]. The thyroid hormone, thyroxine (T4), undergoes conversion to the active form, 3, 3', 5-triiodothyronine (T3), through the action of enzymes called deiodinases (DIO1 and DIO2)[166]. T3 subsequently activates UCP1 transcription in BAT by directly binding to thyroid response elements of genes (TREs) or via binding to PPARγ[167]. Despite high levels of UCP1 expression, BAT-specific knock-out of DIO2 led to significant defects in the processes of lipolysis, lipogenesis, and thermogenesis, consistent with the conclusion that it plays an essential role in maintaining the metabolic functions of BAT[168, 169]. Moreover, oral administration of T4 activates BAT in the cold and at room temperature in rats[170]. Cold also elevated DIO2 expression and T3 levels along with UCP1 levels in BAT[171, 172]**.** Thus, thyroid hormones are crucial players in BAT thermogenesis.

1.3.4 Vascular remodelling/angiogenesis

BAT is highly vascularized to supply oxygen and energy substrates during thermogenesis, and to efflux heated blood from the tissue[56, 173–175]. The vascular density of BAT increases in response to cold exposure via activation of angiogenesis (4°C for 4 weeks) [175, 176]. Amongst all other angiogenic factors, vascular endothelial growth factor (VEGF) is pivotal for BAT expansion during cold exposure[177]. Cold exposure rapidly induces gene expression of pro-angiogenetic factors, vascular endothelial growth factor-B (VEGF-B) and basic fibroblast growth factor (bFGF) in rodents by 2- 3-fold (4°C for 1-4 h) [178]. Vascular endothelial growth factor receptor 2 (VEGFR2) is also important for angiogenesis. Studies have indicated an increase in the expression of VEGFR2 within 2 days of cold exposure[179]. Furthermore, vascular endothelial

growth factor-A (VEGF-A), an isoform of VEGF, also plays a crucial role in mediating angiogenesis during cold exposure (4°C for 5 weeks) [175]. VEGF-A also upregulated the expression of PGC-1α and UCP1 during chronic cold exposure to increase BAT thermogenesis[180]. There are additional isoforms of VEGF, such as vascular endothelial growth factor-120 (VEGF120), that also increase during cold exposure and stimulate BAT proliferation in rats[181]. In contrast, the expression of several anti-angiogenic factors (plasminogen activator inhibitor 1 (PAI1) and pigment epithelium derived factor (PEDF)) that destabilize blood vessels decreases on 2-5 days of cold exposure[179]

1.4 Macroautophagy

Macroautophagy (autophagy) is a quality control process in which a double-membraned vesicle forms around the cellular material to be removed (e.g. damaged organelles) [182]. mTOR is a crucial regulator of several cellular processes, including autophagy. Activated mTORC1 inhibits the formation of mTORC1- Unc-51-like autophagy, activating kinase (ULK1/2) complex to release ULK1 for subsequent activation[183]. Moreover, during conditions of nutritional deprivation, AMP-activated protein kinase (AMPK) inhibits mTORC1 to activate ULK1, Beclin-1, and FoxO3[184]. Upon activation of the kinase activity of (ULK1/2), vacuolar protein sorting 34 (VPS34)/Beclin-1 is recruited to initiate phagophore development[185,186]. During this recruitment process, phosphoinositides are phosphorylated to produce phosphatidylinositol-3-phosphate (PI3P) to expand the phagophore[185, 186]. Several autophagy-related proteins (ATG) are recruited to progress the development of phagophores. ATG4 cleaves light chain 3 pro-(LC3) into LC3-I and subsequently, ATG7 activates LC3-I to transfer to AGT10[186, 187]. Moreover, ATG7 and ATG10 also assemble to form ATG5-ATG12-ATG16L complex that is responsible to link LC3-I to the phosphatidylethanolamine (PE) present on the phagophoric membrane[186, 187]. LC3-I converts to lipidated membrane-bound form (LC3-II) which is thereby cleaved by ATG4 to be recycled[188–190]. Adaptor proteins such as p62/ sequestosome 1 (SQSTM1) recognizes and binds to LC3-II and helps the damaged organelle or protein to sequester within the autophagosome for degradation[188, 191].

1.4.1 Mitophagy

Mitophagy is an organelle-specific autophagy where damaged and excess mitochondria are removed via lysosomal degradation[192]. Various conditions, such as hypoxia, starvation, DNA

damage, dissipated mitochondrial membrane potential, and ROS can initiate mitophagy[193, 194]. There two main mitophagy pathways are 1) ubiquitin-dependent mitophagy and 2) receptor-mediated mitophagy.

1.4.1.1 Ubiquitin-dependent mitophagy

The PTEN-induced kinase 1 (PINK1)/Parkin pathway is the most investigated of the mitophagy pathways[192, 195, 196]. The accumulation of PINK1 on the membrane surface of damaged mitochondria recruits and activates Parkin, a protein that ubiquitinates the mitochondria for recognition by the autophagy machinery[196–199]. Activation of Parkin leads to ubiquitination of proteins like voltage-dependent anion-selective channel 1 (VDAC), mitofusin-2 (MFN2), and mitochondrial fission 1 (FIS1) proteins that further bind to p62[193]. Thereafter, adaptor proteins such as p62 bind polyubiquitinated mitochondria to LC3 to fuse mitochondria with lysosomes[200, 201]. Alongside p62, there are several other adaptor proteins like optineurin (OPTN), nuclear dot protein 52 kDa (NDP52), and Tax1-binding protein 1 (TAX1BP1) that encapsulate mitochondria into autophagosomes[194,202,203].

1.4.1.2 Receptor-mediated mitophagy

Independent receptors like FUN14 domain-containing protein 1 (FUNDC1), adenovirus E1B 19 kDa-interacting protein 3 (BNIP3), and BNIP3-like (NIX) can regulate LC3-mediated mitophagy independent of polyubiquitination[204–206]**.** In response to stress stimuli, BNIP3 and BNIP3L/NIX can localize to the mitochondria to initiate apoptosis[207–211]. Apoptosis is a programmed process of cell death that involves the fragmentation and dysfunction of mitochondria aided by the opening of the mitochondrial permeability transition pore (mPTP)[212]. However, BNIP3 and BNIP3L/NIX can interact with LC3 to encapsulate mitochondria into autophagosomes[205, 206, 213–216]**.** Phosphoglycerate mutase 5 (PGAM5), a glycolytic enzyme, is thought to serve as a molecular switch between mitophagy and apoptosis[217–219]. Specifically, PGAM5 dephosphorylates FUNDC1 to activate mitochondrial fission and mitophagy[217, 218]. Inhibition of FUNDC1-mediated mitophagy reciprocally activates apoptosis by phosphorylating B-cell lymphoma-extra-large (BCL-xL) [217].

1.4.2 Cardiolipin and autophagy/mitophagy

Cardiolipin (CL), a dimeric phospholipid, was first uncovered in the bovine heart in 1942[290]. Despite being discovered initially in the heart, its role is being thoroughly investigated in many cell types and tissues[291, 292]. CL is synthesized in the IMM and is crucial for apoptosis, autophagy/mitophagy and metabolism[291-294]. Moreover, a study showed CL to facilitate fission by influencing the recruitment of Dynamin-1-like protein (DRP1) and by elevating its GTPase activity[295-297]. Thus, in addition to autophagy/mitophagy and apoptosis, CL also plays a pivotal role in maintaining the integrity of mitochondria[295].

Nevertheless, CL found in the IMM might also undergo oxidation to initiate apoptosis[298-301]. This oxidized form of CL (Clox) disrupts the integrity of mitochondrial membrane to promote the formation of mitochondrial membrane pore (MMP)[302]. This is accompanied by the release of cytochrome-c, which in turn triggers caspases to eventually cause cell death[303].

Despite being synthesized in the IMM, some studies have revealed the presence of CL in the outer mitochondrial membrane (OMM) during stress-like conditions[304-306]. As per a study in Hela cells, a decrease in mitophagy was associated with lower levels of CL in the OMM[306]. In contrast, increasing amount of CL in the OMM was found to mediate the recruitment of signaling factors associated with autophagy/mitophagy [302,307-309]. During autophagy/mitophagy LC3 is recruited to the surface of damaged mitochondria to recognize the autophagic cargo for future degradation[306]. This LC3 has hydrophobic pockets whereby CL binds to facilitate the identification of the damaged mitochondria and to maintain mitochondrial health[306, 310]. CL also helps in formation of autophagosomes by interacting with the hydrophobic fingers of the evolutionarily conserved domain (ECD) in Beclin-1[311].

Interestingly, increased levels of CL have also been shown to play an important role in thermogenesis during cold exposure (5°C for 3 weeks) [312]. Acute cold exposure (5°C for 3 days) was shown to increase the levels of CL in BAT of mice as demonstrated through mass spectrometry[312]. Several studies have shown increases in BAT CL levels in rats during chronic cold exposure (5°C for 4 weeks) [313, 314]. Many important questions remain regarding the role of cardiolipin in BAT particularly in relation to the regulation of mitophagy during cold exposure and cold-deacclimation.

1.4.3 Autophagy, mitophagy, and brown adipose tissue

The overall structure of the mitochondrial reticulum impacts substrate oxidation within the cell[220, 221]. Mitochondrial dynamics, including fission and fusion, play crucial roles in adjusting mitochondrial morphology, thereby impacting mitochondrial efficiency and cellular homeostasis[222]

Autophagy prompts the breakdown of the cellular components whereas mitophagy is a type of autophagy that involves the selective degradation of damaged and dysfunctional mitochondria for quality control and maintenance purposes [223,224]. Inhibition of autophagy in 3T3-L1 adipocyte-like cells results in the accumulation of lipid and decreased the protein levels of adipocyte differentiation markers[225]. Additionally, adipocyte-specific knockout of ATG7 increased the rate of fatty acid and β-oxidation in BAT[225]. iBAT specific ATG5 KO mice model exposed to cold (4 °C for 72h) exhibited lower body temperature pointing the importance of autophagy in BAT during cold[226]. Acute cold exposure (4 °C for 72h) showed increase in the protein expression (ATG5, MAP1LC3B, and SQSTM1) of several autophagic genes in BAT[226]. Even chronic cold exposure (4 °C for 7 days) increased the mRNA expression of autophagic genes by 2-fold in BAT[187]. Thus, the upregulation of autophagy during cold exposure might either maintain the thermogenic capacity or might limit nutrient supply to BAT cells potentially impacting thermogenesis. In contrast, decreased expression of several autophagic genes to prevent the removal of BAT mitochondria during thermogenesis has also been reported in response to short-term cold exposure (4 °C for 24 h)[227]. Cairo *et al*. found evidence of protein degradation in BAT during cold-deacclimation and attributed autophagy to be the cause of this process[228]. Moreover, upon transferring mice from cold to thermoneutral temperatures, brown and beige adipose tissues undergo whitening[229]. A study where ATG5 and ATG7 were knocked in BAT and beige adipose tissue, it was noted that autophagy was essential for degrading proteins to convert beige into white adipose tissue[230]. Together, these findings show that autophagy is pivotal for the functioning of BAT.

Mitophagy also recruited proteins like Parkin and dynamin-1-like protein (DNM1L) protein to increase the amount of mitochondrial proteins, mitochondrial turnover, and mitochondrial activity during cold exposure[226]. A study found that mitophagy aided the removal of damaged mitochondria in BAT upon cold exposure (4°C for 72 h) [226]. Moreover, PINK1-null BAT exposed to cold showed the presence of fragmented mitochondria showing that mitophagy was

important for maintaining mitochondrial health[231]. Moreover, BAT of PINK1 KO mice exposed to cold (4°C for 1 week) had decreased OXPHOS capacity and mitochondrial integrity. Mitochondrial fragmentation also stimulated NE mediated uncoupling in brown adipocytes[232]. The role of mitophagy during cold exposure in BAT is a matter of debate, as cold exposure **(**4°C for 3 days) was found to decrease the levels of key mitophagic protein Parkin[213]. Hence, it is pivotal to confirm and gain a deeper understanding of the role of autophagy and mitophagy in BAT.

1.4.4 Traditional and novel methods for the study of mitophagy

Several methods have been used to determine mitophagy in mammalian cells and tissues. Each method has its advantages and limitations. Transmission electron microscopy (TEM) is often used and while it allows analysis of mitochondrial cristae number, width, number, area, and other characteristics of mitochondrial ultrastructure[215, 233], findings do not provide definitive information about mitophagy, and this technique is time consuming, expensive and analyses can be biased by the position of tissue sectioning [234]. Western blot approaches provide more definitive information about mitophagy and quantifies relevant proteins, but can be imprecise and is unable to detect low levels of proteins[235–237]. Moreover, immunohistochemistry of cells or tissues can be used to detect mitophagy by quantifying the colocalization of mitochondria and lysosomes[191, 238, 239]. However, detection of fluorescent signals associated with secondary antibodies challenging[240, 241].

In the past decade, fluorescent transgenic mitophagy reporters have been created to visualize and quantify mitophagy. MitoKiema is used to access mitochondrial turnover/mitophagy in cells and transgenic mouse models[242–244]. Similarly, Mito-timer can be used to monitor mitophagy and biogenesis in fixed and live cells[245–248]. In addition, the mito-QC reporter is a promising approach to determine changes in mitochondrial networks in different tissues as this sensor does not affect mitochondrial structure or function[249, 250]. Mito-QC mice express a pH-sensitive protein that allows analyses of mitophagy flux. This model was created by fusing the mCherry-green fluorescent protein (GFP) tag to FIS1 (a protein in the OMM) [249]. In the absence of mitophagy, mitochondria exhibit red and green fluorescence; however, when a mitochondrion fuses with the lysosome during mitophagy, GFP quenches to emit red fluorescence alone[249]. This mouse model provides an advantage as it can give robust and real-time information about mitophagy in

tissues [249, 250]. It can be used for *in-vivo* studies to provide insights into mitochondrial health[249]. Apart from quantifying mitophagy events, this model is compatible with several techniques, including flow cytometry, immunofluorescence, and live-cell imaging[249–251]. However, caution must be taken when handling Mito-QC mouse samples to prevent any shift in pH sensitivity in fluorescent signals[249].

1.4.5 Effect of cold-deacclimation on BAT autophagy

Cold-deacclimation is a process that is induced when a cold-adapted animal is exposed to warmer temperatures. During cold-deacclimation, NST in BAT is shut down as it is no longer needed. Limited information is available regarding the mechanisms induced in BAT during cold-deacclimation.

In the past, the effects of cold-deacclimation in mice were studied by acclimating mice to cold (4°C for 4 weeks) with denervation of the ventral and lateral nerves entering iBAT [252]. This study revealed that several morphological changes occur in BAT during cold-deacclimation where BAT turns pales in colour, size of mitochondria decreases and BAT lipid content increases[252]. Denervation of BAT decreases the wet weight of BAT by 25-45%[253], accompanied by a 50% decrease in BAT proteins after 14 days[253]. Similarly, iBAT total protein content was found to decrease by 25% and 50% after 1 or 7 days of cold-deacclimation, respectively[228]. The decrease in iBAT protein content during cold-deacclimation is accompanied by decreases in BAT mitochondrial content[252–254].

When mice were transferred from a cold-adapted state (4°C, 21d) to a thermoneutral temperature (29°C, 1 d), mRNA expression of UCP1 decreased by 70% in 24 hours[228]. Following 7 days of cold-deacclimation, the relative transcript levels of UCP1 further decreased by ~90%[228]. No significant difference in the amount of UCP1 was seen after 24 h of denervation, but UCP1 decreased by 47% 7 days after denervation[253]. UCP1 has a long half-life of 20-100 h [255]. In contrast to UCP1, other mitochondrial proteins are rapidly degraded within 24 hours of cold-deacclimation, including several subunits of complex I, II, IV, and V[228]. However, the ratio of mtDNA/nDNA during cold-deacclimation was not altered[228].

The mRNA expression of FGF21 which is responsible for differentiation and angiogenesis in BAT decreases when mice are exposed to cold-deacclimation[228]. This might indicate that angiogenesis

and adipogenesis decrease during cold-deacclimation although more research is needed. PGC1α also decreases following only 24 hours of cold-deacclimation. Observations by TEM detected the presence of mitochondria with fragmented cristae and autophagosomes during 7 days of cold-deacclimation in BAT[228]. Following one day of cold-deacclimation, there were increased levels of Parkin, PINK1, and LC3 consistent with increased mitophagy in BAT[228]. Moreover, Parkin KO mice subjected to cold-deacclimation exhibited defects in BAT mitophagy providing evidence that Parkin was an important regulator of mitophagy in BAT[228].

1.5 Rationale

BAT plays an essential role in thermoregulation and undergoes remodelling to adapt to the changes in the temperature of the external environment. As reviewed above, environmental cold stimulates BAT activation and growth, leading to enhanced capacities for BAT thermogenesis and whole-body thermoregulation. On transitioning to warm temperatures, BAT undergoes changes in activity, structure, and content. To better understand the dynamic nature of BAT, we embarked on cold-deacclimation studies that explored changes in BAT when a cold-adapted mouse adjusts to thermoneutrality (at time points up to 48h). Specifically, we sought to examine any changes in autophagy and mitophagy during cold de-acclimation.

1.6 Overall Aim

To investigate alterations in the whole-body bioenergetics, and BAT activity, structure and content in mice during the acute transition from cold-acclimation to deacclimation.

1.7 Hypothesis

We hypothesized that cold-deacclimation (up to 48h) in mice would decrease whole body and BAT energy expenditure, and decrease BAT mitochondrial structure and content, due to increased mitophagy.

2 Methods

2.1 Animals

All experiments involving mice were approved by the Animal Care Committee of the University of Ottawa granted and conducted according to the guidelines and principles of the Canadian Council of Animal Care Studies were conducted on male and female C57BL/6J and Mito-QC mice (gift from Dr. Yan Burelle, University of Ottawa) aged 7-9 weeks. Mice were housed individually in ventilated cages with a 12/12 h light-dark cycle (6 AM-6 PM) and fed a standard chow diet (44.2% carbohydrates, 6.2% fat, and 18.6% crude protein (T.2018-Harlan)). Unless otherwise indicated, mice were acclimated to cold (4°C) for 7 days and subsequently sacrificed (T0) or returned to thermoneutrality (30°C) for 3, 12, 24, or 48 hours (T3, T12, T24, and T48, respectively). Mice were sacrificed by cervical dislocation, and iBAT was isolated and used immediately for high-resolution respirometry, fixed for microscopy, or snap-frozen and stored at -80°C for further analysis.

2.2 Body composition and mouse calorimetry

Twelve C57BL/6J mice were randomly selected to determine changes in whole-body energetics over 5 days of cold-deacclimation. Fat and lean body mass was determined using a magnetic resonance imaging whole-body composition analyzer (EchoMRI, Houston, TX). The rates of whole-body oxygen consumption (VO2), carbon-di-oxide production (VCO2), and respiratory exchange ratio (RER) was measured every 26 minutes during cold-deacclimation using a 12-chamber Comprehensive Lab Animal Monitoring System (CLAMS) system (Oxymax, Columbus Instruments, OH). Moreover, to further analyze data, we applied a percentage relative cumulative frequency (PRCF) approach to determine the differences in energy expenditure during cold exposure and cold-deacclimation[256]. Mice were acclimated at 4°C for 3 days and then for 5 days in the CLAMS chambers (equipped with cotton nestlets) prior to collection of data for analyses. Readings were recorded prior to and following the elevation in temperature to 30°C (for the next 5 days).

2.3 Isolation of BAT mitochondria

iBAT dissected from C57BL/6J mice was minced in isolation buffer (70 mM sucrose, 210 mM

mannitol, 5 mM HEPES, 1 mM EGTA, and 1% fatty acid- free BSA), and subsequently homogenized using a Potter Elvehjem teflon–glass tissue grinder. The homogenate was transferred to a 1.5 mL tube and centrifuged at 800xg for 10 minutes at 4°C. The supernatant was transferred to a fresh 1.5 mL tube and centrifuged at 8500xg for 10 min to obtain the mitochondrial pellet. The mitochondrial pellet was washed in a buffer containing 0.5% BSA and 0.25 M sucrose, then centrifuged at 8500xg for 10 minutes. The purified mitochondrial pellet was gently resuspended in the isolation buffer. Protein content was measured by Bradford assay and mitochondria were then used for high-resolution respirometry (HRR) or western blotting.

2.4 High-resolution respirometry

Mitochondrial respiratory function was determined using an Oxygraph-2k system (O2k; Oroboros, Innsbruck, Austria) in permeabilized BAT explants and isolated mitochondria. For assessments of permeabilized tissue, iBAT was cleaned, minced, and placed into ice-cold BIOPS buffer (2.77 mM CaK_2 EGTA, 7.23 mM K_2EGTA,10 mM imidazole, 20 mM taurine, 50 mM K-MES, 0.5 mM dithiothreitol, 6.56 mM MgCl2, 5.77 mM ATP,15 mM creatine phosphate) containing 50 µg/ml saponin to permeabilized the iBAT for 30 min at 4°C to permeabilize the explants. The explants were washed thoroughly (3X) in mitochondrial respiration medium (MiR05) (0.5 mM EGTA, 3 mM $MgCl_2{*}6H_2O$, 20 mM taurine, 10 mM KH_2PO_4, 20 mM N-2-hydroxyethylpiperazine-N-2-ethane sulfonic acid, 110 mM d-sucrose, 0.1% bovine serum albumin and 60 mM lactobionic acid; pH 7.1). Rates were determined by adding 2-5mg of iBAT to the Oroboros chambers containing 2 ml of MiR05. All measurements were performed at 37°C, and the Oxygraph-2k units were calibrated. Respiratory rates of 50µg isolated BAT mitochondria were also assessed.

The experimental protocol began with the addition of 0.1mM palmitoyl-carnitine (p-car), to activate UCP1 and 5µM oligomycin to inhibit the F_O subunit of ATP synthase to assess leak respiration. Next, 5mM pyruvate, 2mM malate, and 10mM glutamate were added to the chambers to support complex-I linked respiration. Following this, 10mM succinate was added to support complex-II mediated respiration and 5mM glycerol 3-phosphate (G3P) was added to feed electrons to the ubiquinone pool to aid complex-III mediated respiration. In the end, the protonophore 0.5µM carbonyl cyanide p-trifluoro-methoxyphenyl hydrazone (FCCP) was added to obtain maximum mitochondrial capacity. Respiration rates were normalized to the weight of tissue for BAT explant analyses or to mg protein for analyses of isolated mitochondria.

2.5 Confocal microscopy

Mito-QC mice were sacrificed, and iBAT was dissected, preserved, and fixed in 4% paraformaldehyde solution (pH=7.4) for 2 days. On day 3, iBAT was transferred to a 1 ml mini tube filled with 30% sucrose (pH=7.4) for 24 hours at 4°C. iBAT was dried and snap-frozen in cold isopentane following sectioning by a microtome. The 10μm-thick frozen iBAT section was mounted with ProLong™ Diamond antifade mountant with DAPI stain (Thermofisher #_P36962). The GFP and the mCherry signals were detected by an LSM 880 Airyscan (Zeiss AxioObserverZ1(inverted)) in mito-QC BAT sections. The number of mitolysosomes was quantified in mito-QC mice using the Mito-QC counter on FIJI (Image J; NIH).

2.6 Mitochondrial ultrastructure analysis by transmission electron microscopy

Approximately 10mg of iBAT from mice exposed to cold-deacclimation was dissected quickly and was fixed in 2.5% glutaraldehyde in 0.1M sodium cacodylate buffer at pH 7.4. The tissue samples were subjected to gentle rocking overnight at 4°C. The McGill Facility for Electron Microscopy personnel handled the preparation and TEM imaging of these BAT samples. The samples were fixed in 1% aqueous OsO4 +1.5% aqueous potassium ferrocyanide and then subjected to washing. Further, the samples were dehydrated, embedded in 100% Epon, and then polymerized. The samples were sectioned (90-100nm), transferred to a 200-mesh copper grid, and stained with 4% uranyl acetate and Reynold's lead. The grids were imaged by an FEI Tecnai G2 spirit 120 kV TEM equipped with a Gatan Ultrascan 4000 CCD camera (Model 895). The images obtained at 2000X (2K) in the form of Digital Micrograph 16-bit images (DM3) were converted to TIFF images for quantification on FIJI (Image J; NIH). The acquired images were used to quantify the number of mitochondria, mitochondrial area, number of lipid droplets, size of lipid droplets, number of cristae, length of cristae, and volume of cristae in BAT sections from mice exposed to several timepoints of cold-deacclimation. Quantification was done manually using freehand selection as per Lam *et al.*[257].

2.7 Western blots

Frozen BAT explants (50-60mg) from mice exposed to several timepoints (T0-T48) were weighed and homogenized with ice-cold Radio-Immunoprecipitation assay buffer (RIPA, Millipore) mixed with protease and phosphatase inhibitors (Sigma Aldrich; P8340). Following sonication, tissues were mechanically homogenized in a Potter Elvehjem Teflon-glass grinder.

BAT homogenates were centrifuged at 14,000xg for 10 minutes at 4°C to remove excessive fat residues. The homogenate protein concentration was determined by BCA assay using a commercially available kit according to the manufacturer's protocol (ThermoFisher Scientific #23235).

10-20μg of protein samples were loaded on SDS-polyacrylamide gel (8-15% gels). After electrophoresis, the proteins were transferred to a polyvinylidene fluoride (PVDF) membrane. The membrane was blocked for an hour in 5% bovine serum albumin (BSA). The membranes were incubated overnight in the following primary antibodies at several dilutions: UCP1 antibody (1:2000; Sigma Aldrich, #U6382), total OXPHOS rodent cocktail (1:1000; Abcam, #Ab110413), LC3A/B (1:2000; Cell Signaling Technology, #127415), Parkin (1:1000; Santa Cruz, #sc-32282), FUNDC1 (Proteintech #28519-1-ap), Beclin-1 (1:2000; Proteintech, #13762) OPA-1 (1:2000; Abcam, #Ab9833), MFN1 (1:2000; Abcam, #Ab126575), MFN2 (1:2000; Abcam, #A56389), Fis1 (1:1000; BioVision, #42364). The next day, the membrane was washed 5X with TBS-T and probed with their respective secondary antibody (1:5000) for 60 mins. Membranes were washed 5X in TBS-T and were imaged on ChemiDoc™ MP Imaging System (Bio-Rad). The protein bands were visualized, quantified, and normalized to Coomassie stain or to a housekeeping protein using FIJI (Image J; NIH).

2.8 Real-time quantitative PCR

DNA was extracted from iBAT as per Guo *et al.*[258.] The tissue was mixed with DNA lysis buffer (1M Tris, 5mM EDTA, 0.2% SDS, 200mM NaCl, pH=8) and homogenized using a Potter Elvehjem teflon–glass tissue homogenizer, Next, proteinase K solution was added to protein lysates in 1 ml mini tube and was incubated overnight at 55 °C. Thereafter, DNA was extracted using phenol/chloroform/isoamyl alcohol (25:24:1) and centrifuged (16000xg for 10 min) to collect the supernatant. Cold isopropanol was added to the supernatant, incubated overnight at -20°C and subsequently centrifuged (16000xg for 10 min). The supernatant was mixed with cold 70% alcohol, spun and dried to obtain the DNA pellet. The pellet was dissolved in 0.4 ml tris-EDTA (TE) buffer and the concentration and quality of mitochondrial DNA (mtDNA) were measured using NanoDrop 2000 (Thermo Scientific). The concentration of mtDNA and nuclear DNA (nDNA) was measured by mixing the master mix (the combination of forward and reverse primers) with the SYBR mix. The primers of mtDNA and nDNA used for this assay are listed in Table 1.

Gene	Forward	Reverse
Mitochondrial	5'-TGC TAG CCG CAG GCA TTA C-3'	5'-GGG TGC CCA AAG AAT CAG AAC-3'
Nuclear	5'-CTT CCC CAC TGG CCT CAA G-3'	5'-CCA AAA CCC AGT GAT CCA GC-3'

Table 1 Primer Sequences used for quantitative RT-PCR

2.9 Statistical analysis

All statistical tests in our study were performed on GraphPad Prism 9 (GraphPad Prism, La Jolla, CA, USA). One-way ANOVA with post hoc Tukey's test was used to compare the differences between several timepoints of cold-deacclimation. The data in the study are presented as mean ± SD, and statistical significance is defined as $p < 0.05$.

3 Results

3.1 Whole-body energy expenditure decreases during cold-deacclimation

To measure the changes in energy expenditure during cold-deacclimation, mice were acclimated to 4^{o}C (T0) in the CLAMS system before increasing the temperature to 30°C (T3-T120). We began the experiment by measuring the changes in the food intake of mice exposed to several timepoints of cold-deacclimation. In this experiment we collected data beyond the 48h time point of cold-deacclimation, extending to 120h. As expected, daily food intake of mice decreased over 120 hours (Figure 1A, $p<0.0001$ at all timepoints). Next, we compared the changes in overall oxygen consumption (VO2) during cold exposure and cold-deacclimation. Interestingly, there was a 66% decrease in whole-body oxygen consumption (T3-T120) compared to T0 (Figure 1B, $p<0.0001$ for all timepoints). The RER initially increased during T12-T72 (Figure 1D, $p<0.0001$ for T12-T48, $p<0.001$ for T72) with subsequent decrease at T120 (Figure 1D, $p<0.001$) when compared to T0.

The PRCF approach was used to determine whether differences between VO2 and RER were driven by changes at the lower or higher range of values collected over time in the CLAMS system, as described by Riachi *et al.*[256]. The PRCF approach analyzed large VO2 datasets of the two groups, and VO2 was found to be lower during cold-deacclimation (T3-T120) when compared to cold (T0) (Figure 1C). Next, we determined RER an estimate of the respiratory quotient (RQ) to help identify any difference in the type of energy source oxidized by the mice. On determining the 50th percentile of the PRCF curve, we discovered that the RER value at T0 and T3-T120 was 0.935 and 1.06, respectively (Figure 1E). RER of 0.935 and 1.06 indicates mice exposed to cold oxidized carbohydrates as a fuel source (Figure 1E), consistent with an anabolic (eg lipid synthesis) rather than a catabolic state overall in mice[259–261].

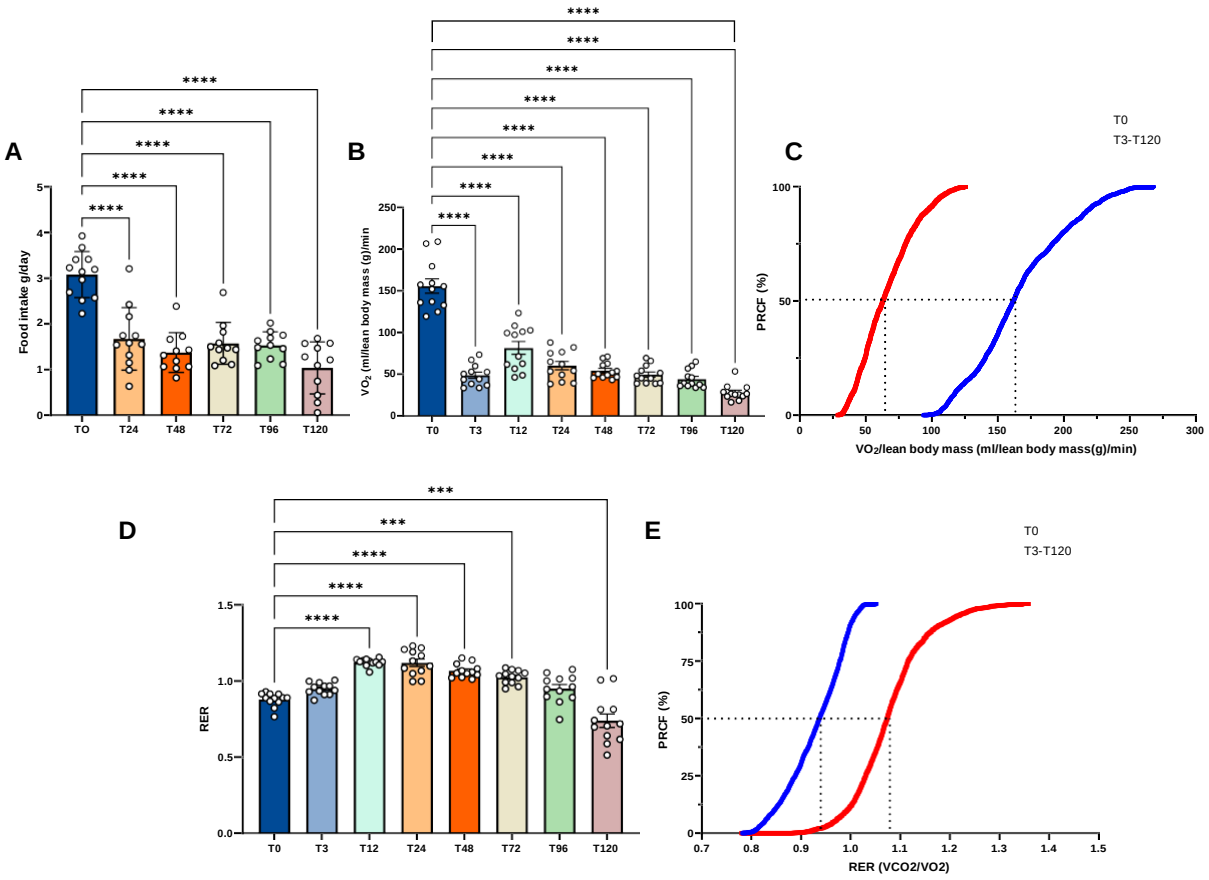

Figure 1. Whole-body energy expenditure decreases during 3-120h of cold-deacclimation.

C57BL/6J mice were were acclimated at 4°C for 3 days with subsequent acclimation for 5 days in the CLAMS (T0) and then housed at 30°C for 3,12, 24, 48, 72, 96, and 120 hours (T3, T12, T24, T48, T72, T96, T120) A) Daily food intake. B) VO_2 consumption was measured and normalized to lead body mass. C) The difference in VO2 between mice at T0 and the mice at T3-T120 are shown via PRCF plots of VO_2 D) Respiratory exchange ratio (RER) was determined at E) The difference in RER between mice at T0 and those at T3-T120 are shown via PRCF plots of RER. (n=12 biologically independent samples/group). Comparisons are made with one-way ANOVA with post hoc Tukey's test; data are presented as mean ± SD. ***=p<0.001, ****=p<0.0001.

3.2 Metabolic capacity of BAT explants and isolated mitochondria decreases within 3-48 h of cold-deacclimation.

Analysis of BAT explants using high-resolution respirometry showed Complex-I mediated respiration was lower at T24-T48 compared to T0 (Figure 2A) ($p<0.001$ at T24 and $p<0.01$ at T48). Additionally, Complex I+II mediated leak, measured by the addition of succinate, was decreased at T48 (Figure 2B) ($p<0.05$) as compared to T0. We measured G3P-mediated leak respiration in both groups, and a decrease was observed at T3-T48 (Figure 2C) ($p<0.05$ at T3 and T24 and $p<0.001$ at T48) as compared to T0.

Further, we determined the impact of cold-deacclimation on the respiratory capacity of isolated mitochondria from BAT. Mitochondria were used to eliminate the interference of blood vessels, macrophages, and exosomes that could affect the changes in the respiratory capacity of BAT. Interestingly, complex I+II and G3P-supported leak respiration were decreased at T48 (Figure 2E, F) ($p<0.05$ for complex I+II leak and $p<0.01$ for G3P-supported leak) as compared to T0. No changes were observed in complex I-mediated respiration during cold-deacclimation, unlike BAT explants (Figure 2D). Taken together, the metabolic capacity of mitochondria decreased after 48 hours of cold- deacclimation.

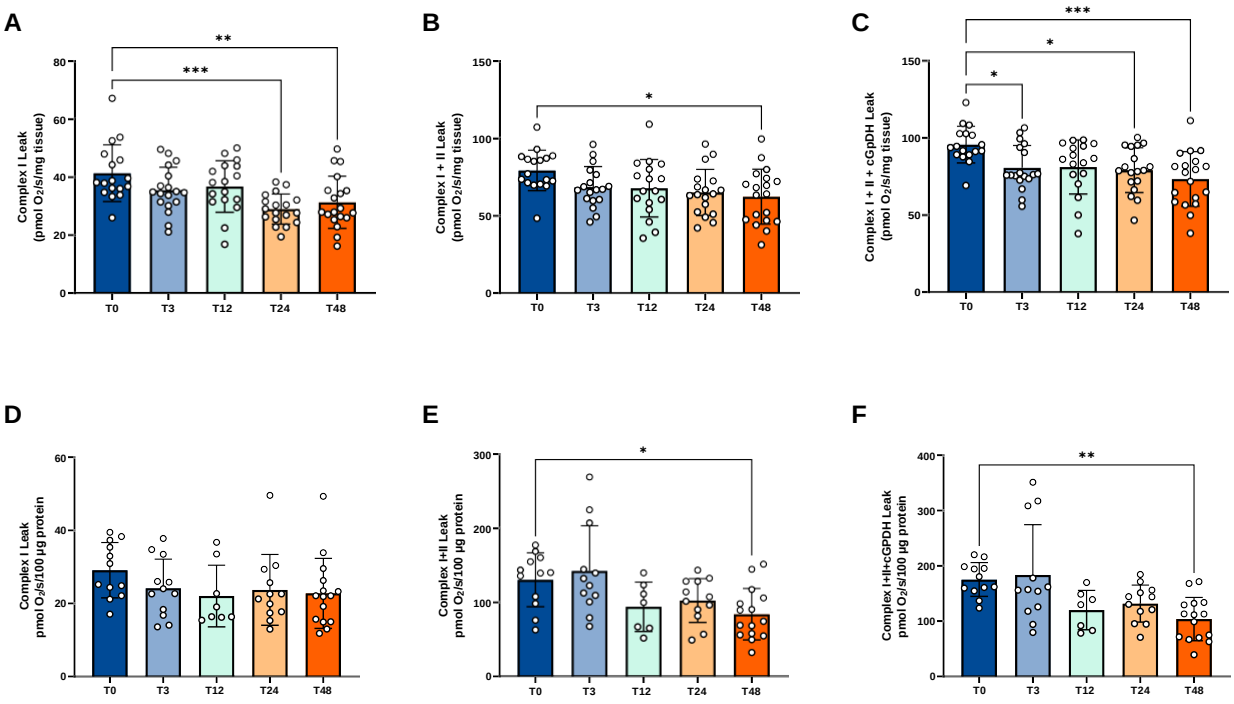

Figure 2. Metabolic capacity of BAT explants and isolated mitochondria decreases within 3-48 h of cold-deacclimation.

Mitochondrial respiration was measure by HRR in BAT explants (A-C) or isolated mitochondria (D-F) from from C57BL/6J mice acclimated at 4°C for 7 days (T0) and then housed at 30°C for 3,12, 24 and 48 hours (T3, T12, T24, T48) A) Complex I mediated leak, B) Complex I+II leak C) Complex I+ II+ cGPDH leak (n=17-19 biologically independent samples/group) D) Complex I mediated leak E) Complex I+II leak F) Complex I+ II+ cGPDH leak (n=8-12 biologically independent samples/group). Comparisons are made with one-way ANOVA with post hoc Tukey's test; data are presented as mean ± SD.*=p<0.05, **=p<0.01. ***=p<0.001.

3.3 BAT mitochondrial content decreases within 12 h of cold-deacclimation

After we carried out the functional studies in mitochondria, we decided to determine changes in the total protein and mitochondrial content upon cold-deacclimation. A 22% decline in total proteins was observed per mg of tissue at T48 as compared to T0 (Figure 3A) ($p<0.001$). Moreover, a time-dependent decrease in the total protein content was also observed during cold-deacclimation (Figure 3A) ($p=0.0001$).

When normalizing mitochondrial yield to the total tissue weight, mitochondrial proteins were significantly decreased within 12 h of cold-deacclimation (Figure 3B) ($p<0.05$ for mitochondrial protein/tissue weight at T12-T24 and $p<0.01$ at T48). We also determined mitochondrial content by the widely used mtDNA assay to confirm our observation. Using qPCR, mtDNA:nDNA was determined, and a significant decline was observed at T24-T48 (Figure 3C) ($p<0.05$ at T24 and $p<0.00001$ at T48) as compared to T0. Taken together, total protein content in BAT decreased with increasing cold-deacclimation time, whereas mitochondrial content decreased within twelve hours of cold-deacclimation.

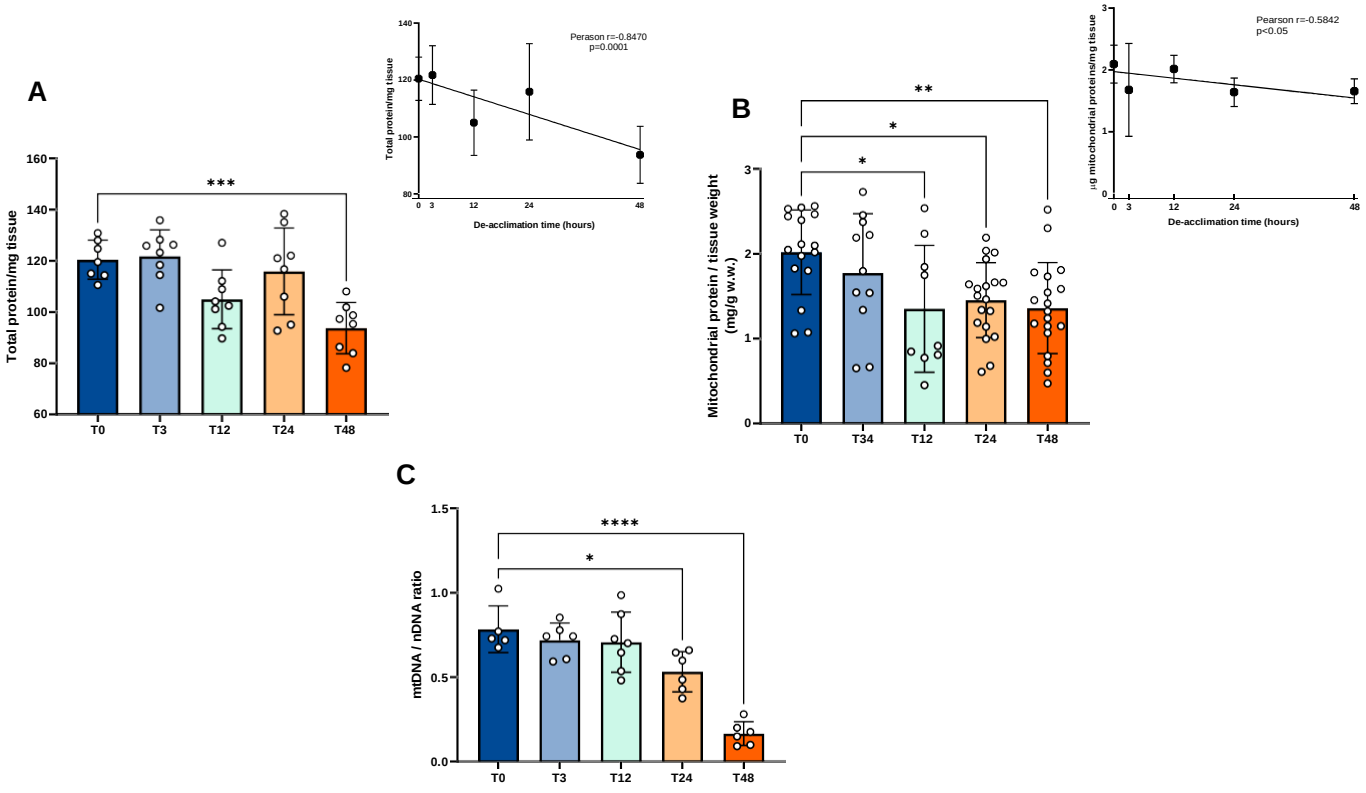

Figure 3. BAT mitochondrial content decreases within 12 h of cold-deacclimation.

C57BL6/J WT mice were cold acclimated at 4°C for 7 days and then housed at 30°C for 3,12, 24, and 48 hours. A) Total protein content was demonstrated by total protein per wet weight tissue. (n=7-8 biologically independent samples/group). B) Mitochondrial protein content was demonstrated by mitochondrial yield per wet-weight tissue. (n=10-19 biologically independent samples/group). (c) mtDNA copy number (mtDNA/nDNA) was measured by qRT-PCR. (n=5-7 biologically independent samples/ group). Comparisons are made with one-way ANOVA with post hoc Tukey's test; data are presented as mean ± SD.*p<0.05, **p<0.01, ***=p<0.001, ****=p<0.0001.

3.4 Expression levels of complex II and III proteins decrease in BAT during cold-deacclimation

A decrease in mitochondrial yield during cold-deacclimation indicates low amounts of mitochondrial proteins. Thus, we determined the changes in significant protein expression in mitochondria like UCP1 and OXPHOS complexes. Although we expected to observe a decrease in UCP1 expression during cold-deacclimation, we did not see any changes (Figure 4B). Similarly, the amount of UCP1 protein per BAT depot was calculated as per Kalinovich *et al.*[262] and no changes were noted in UCP1 expression during cold-deacclimation (Figure 4C).

Immunoblot analysis of key OXPHOS proteins revealed that Complex II decreased at T48 compared to T12 (Figure 5B, $p<0.05$), whereas no changes were observed in complex I, II, IV, and V expression during cold-deacclimation (Figure 5B). Furthermore, we measured the OXPHOS proteins in the total BAT depot as per Kalinovich *et al.* [262]. Expression levels of Complex I and II proteins were decreased at T48 when compared to T12 and T0 respectively (Figure 5C) ($p<0.05$ for complex I) ($p<0.05$ for Complex II at T48 compared to T0 and $p< 0.01$ for Complex II T48 compared to T3). A time-dependent decrease was observed in complex III expression during cold-deacclimation (Figure 5C, $p=0.0589$).

Overall, these results support the conclusion that protein levels of complex II and III decrease during cold-deacclimation.

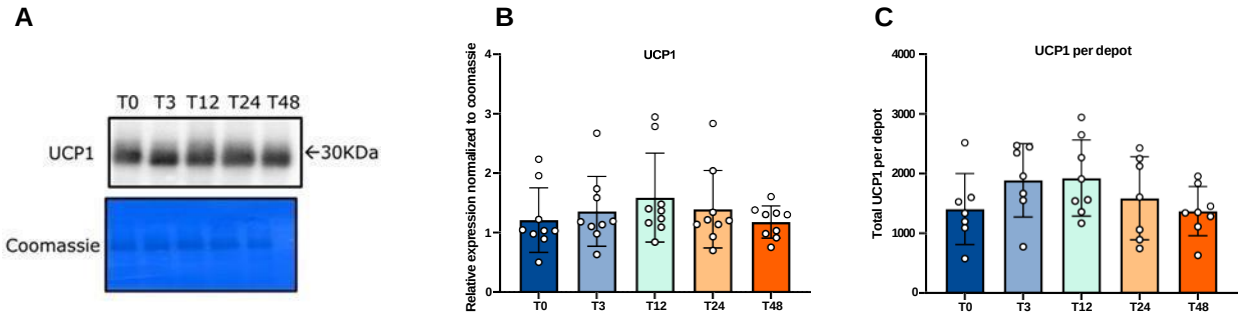

Figure 4. UCP1 protein expression does not change over 48h of cold-deacclimation.

Western blot images of UCP1 bands in iBAT from C57BL/6J mice acclimated to 4°C for 7 days and then housed at 30°C for 3,12, 24, and 48 hours. Coomassie staining of proteins was used as the loading control. B) Densitometry analysis of UCP1 expression from (A). C) Total amounts of UCP1 in iBAT tissue were obtained by multiplying the amount of UCP1 in BAT with the total amount of mitochondrial proteins (Fig 4(B)) per mg tissue (Fig 3(A)). (n=6-8 biologically independent samples/group). Comparisons are made with one-way ANOVA with post hoc Tukey's test; data are presented as mean ± SD.

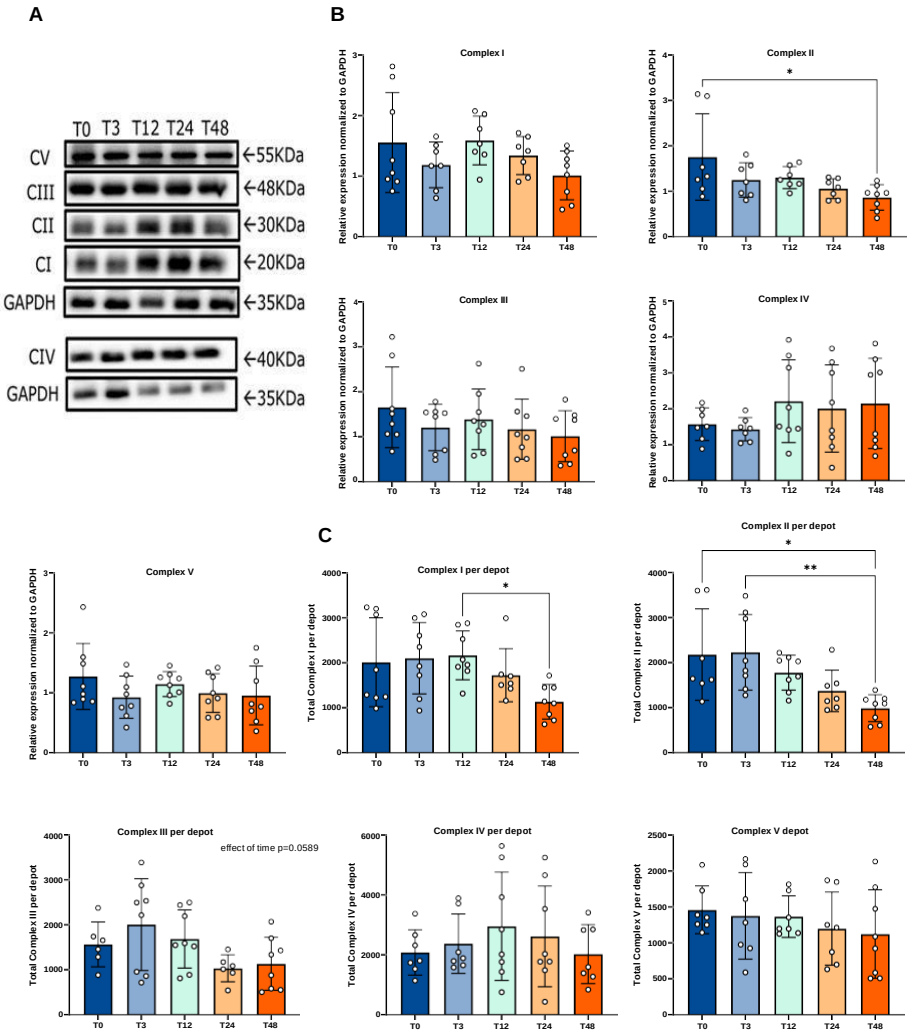

Figure 5. Expression levels of complexes II and III decrease in BAT during cold-deacclimation

A) Western blots of complexes I-IV in iBAT from C57BL/6J mice acclimated to 4°C for 7 days and then housed at 30°C for 3,12, 24, and 48 hours. GAPDH was used as the loading control. B) Densitometry analysis of complexes I-IV expression in iBAT as in (A). C) Total amounts of OXPHOS proteins in iBAT were obtained by multiplying the amount of OXPHOS proteins in BAT with the total amount of mitochondrial proteins (Fig 4(B)) per mg tissue (Fig 3(A)). (n=6-8 biologically independent samples/group). Comparisons are made with one-way ANOVA with post hoc Tukey's test; data are presented as mean ± SD.*$p<0.05$, **$p<0.01$.

3.5 Mitophagy increases in iBAT within 48 h of cold-deacclimation

We used western blots to quantify the protein levels of the autophagic/mitophagy markers, Parkin, LC3, and Beclin, and no changes were observed (Figure 6). However, a 50% decrease was observed in the protein level of FUNDC1 at T48 (Figure 6, $p<0.05$). This decrease in FUNDC1 expression during cold-deacclimation suggests a reduction in mitophagy/autophagy. To accurately visualize mitophagy in BAT during cold-deacclimation, we quantified the number of mitolysosomes using mito-QC reporter mice, as shown in Figure 7A. The red punctae were automatically quantified by a mito-QC *counter* in iBAT from mice exposed at T0-T48, and an increase in mitophagy was observed. As mitochondrial content decreased during cold-deacclimation (Figure 3), we normalized our results to mitochondrial content. Our results were in alignment with our hypothesis, were we observed an increase in the number of mitolysosomes at T48 (Figure 7C ($p<0.05$)). Additionally, we also observed an increase in mitolysosomes at T48 (Figure 7D ($p<0.05$)).

Overall, we observed a decrease in FUNDC1 levels and an increase in mitophagy within 48h of cold-deacclimation.

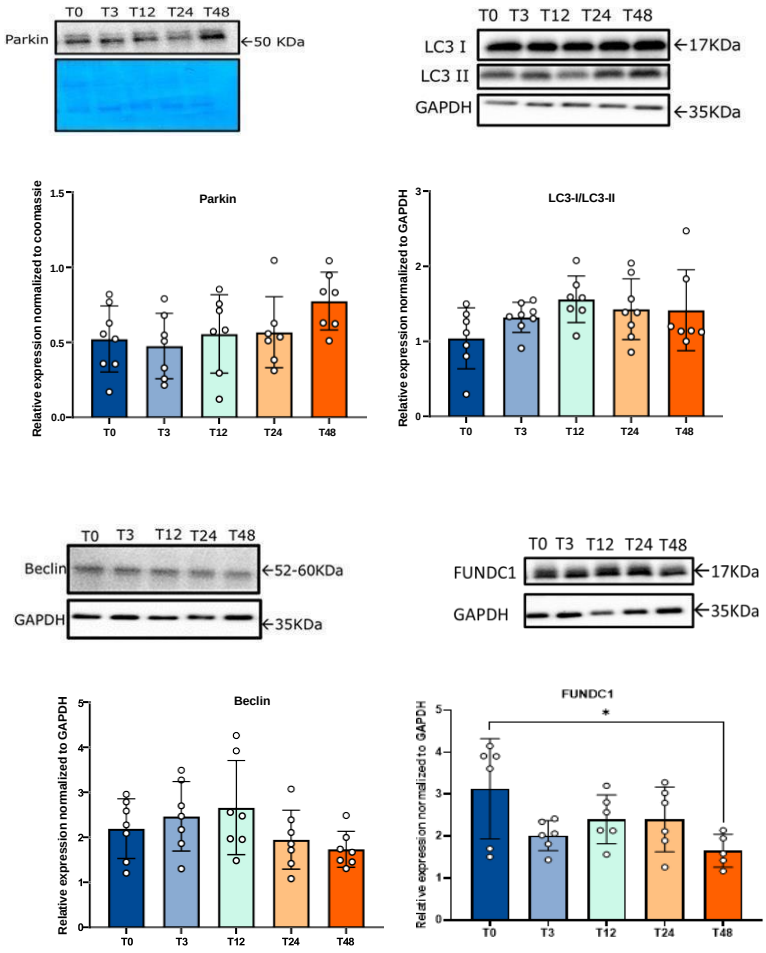

Figure 6. Mitophagic marker FUNDC1 decreases in iBAT at 48h.

Western blot images and densitometry analysis of Parkin, LC3I/LC3II, Beclin and FUNDC1 in iBAT from C57BL/6J mice acclimated to 4°C for 7 days and then housed at 30^0C for 3,12, 24 and 48 hours. Coomassie or GAPDH was used as a loading control. (n=6-8 biologically independent samples/group) Comparisons were made with one-way ANOVA with post hoc Tukey's test; data are presented as mean ± SD.*=p<0.053.6 Changes in BAT mitochondrial ultrastructure within 24-48h of cold-deacclimation.

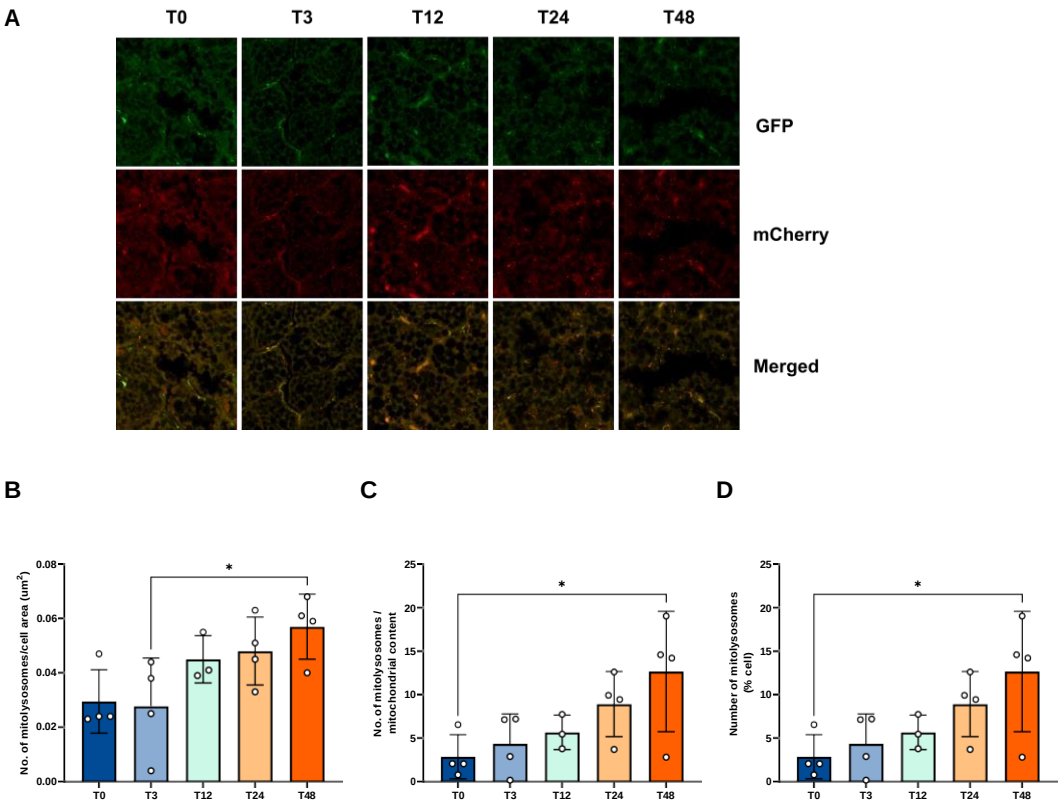

Figure 7. Mito-QC mice models show increased mitophagy in iBAT within 48 h

A) Representative confocal images of iBAT of mito-QC mice at various cold-deacclimation time points. Yellow punctae indicate normal mitochondria (mCherry+ GFP+). Red punctae indicate mitochondria fusing with lysosomes and undergoing mitophagy (mCherry+; GFP quenched). B) Total number of mitolysosomes counted per cell area defined by the manual selection of ROIs. C) Total number of mitolysosomes counted per mitochondrial content. D) The percentage of mitolysosomes in BAT in the cell. Quantification was performed with the following parameters: Radius for smoothing images = 1; Ratio threshold = 0.4; Red channel threshold = 0.6 (n=3-4 biologically independent samples/ group). Comparisons were made with one-way ANOVA with post hoc Tukey's test; data are presented as mean ± SD.*=$p<0.05$.

3.6 Changes in BAT mitochondrial ultrastructure within 24-48h of cold-deacclimation

We next examined the ultrastructure and cristae morphology of BAT mitochondria using TEM. First, we determined the changes in the lipid droplet area and number. Findings demonstrated an increase in lipid area at T48 (Figure 8C) ($p<0.01$) as compared to T0. Results also indicated a decrease in the number of lipid droplets at T24-T48 (Figure 8B) ($p<0.05$ for all time points).

Quantification of TEM micrographs revealed no change in the number of mitochondria (Figure 8D); however, mitochondrial area (as % of cytoplasm) was decreased at T48 (Figure 8E) ($p<0.05$), consistent with findings in Figure 3. While it appears that there may an increase in the number and size of glycogen granules with cold-deacclimation, this was not quantified.

An increase was observed in the average cristae length at T24-T48 as compared to T3 (Figure 8G) ($p<0.05$ at T24 and $p<0.01$ at T48). Furthermore, cristae number increased at T48 as compared to T3 (Figure 8F) ($p<0.05$)). Cristae volume decreased at T3-T24 compared to T0 (Figure 8I) ($p<0.05$). However, no changes were observed in the average cristae area during cold-deacclimation (Figure 8H).

Taken together, the process of cold-deacclimation leads to BAT lipid accumulation, a decrease in lipid droplet number, mitochondrial fragmentation, and decrease in mitochondrial cristae volume.

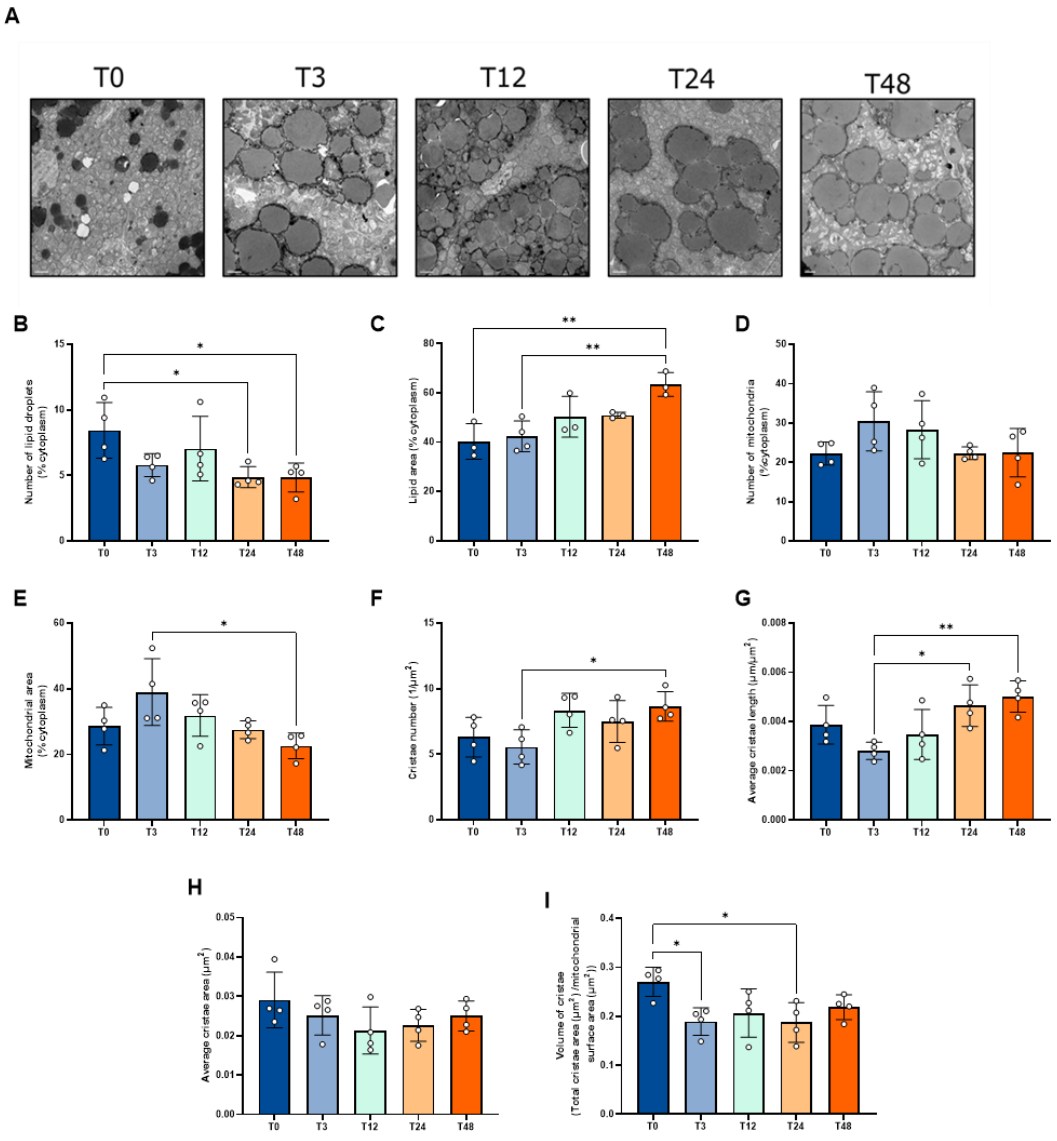

Figure 8. Changes in BAT mitochondrial ultrastructure within 24-48h of cold-deacclimation

A) TEM images of BAT tissues from C57BL6/J WT mice acclimated to 4°C for 7 days and then housed at 30°C for 3,12, 24, and 48 hours. B) Quantification of lipid droplet number C) Quantification of lipid droplet size (n=3-4 biologically independent samples/group, 10 micrographs were analyzed for each mouse) D) Quantification of number of mitochondria E) Quantification of mitochondrial area F) Quantification of cristae number G) Quantification of average cristae length H) Quantification of average cristae area I) Quantification of volume of cristae. (n=4 biologically independent samples /group, 5 micrographs were analyzed for each

mouse). Comparisons are made with one-way ANOVA with post hoc Tukey's test; data are presented as mean ± SD.*$p<0.05$, **$p<0.01$.

3.7 Alteration in mitochondrial dynamics occurs during cold-deacclimation

Based on our TEM findings, we speculated that there were increases in mitochondrial fragmentation during cold-deacclimation. This process is necessary to sustain the presence of healthy mitochondria and facilitate mitochondrial turnover during cold-deacclimation.

Western blots were used to measure levels of mitochondrial fusion proteins (OPA1 and MFN1, and MFN2) and mitochondrial fission protein, FIS1. Interestingly, the expression of proteins OPA1, MFN2, or FIS1 did not change during cold-deacclimation (Figure 9). However, our results indicate a decrease in the expression of MFN1 during cold-deacclimation, as shown in Figure 9 ($p<0.05$).

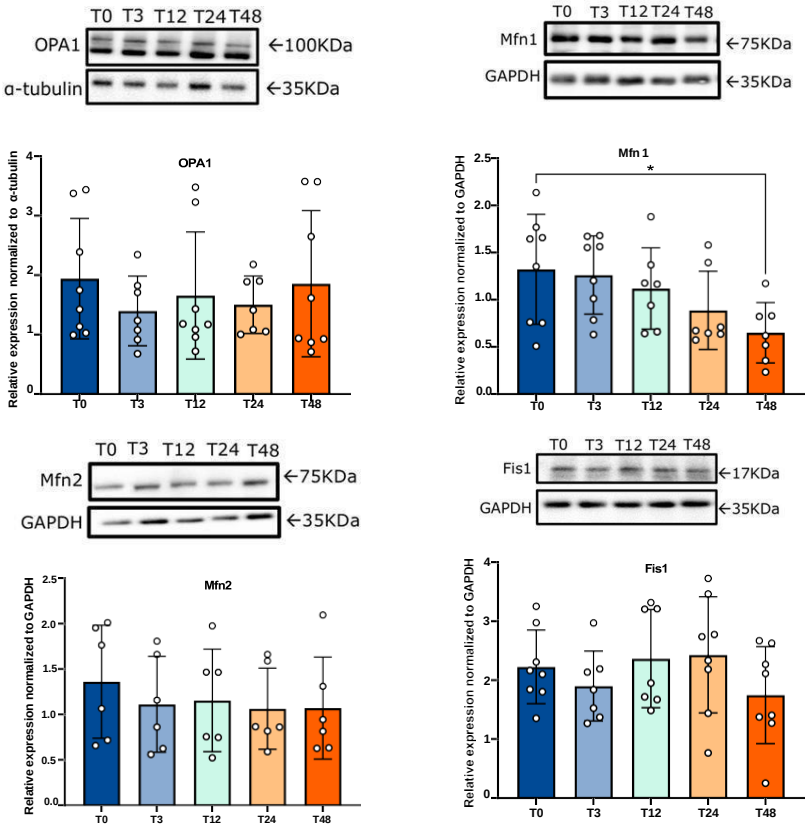

Figure 9. Alteration in protein markers of mitochondrial dynamics during cold-deacclimation

Western blot images and densitometry analysis of OPA1, MFN1, MFN2 and FIS1 in iBAT from C57BL/6J mice acclimated to 4°C for 7 days and then housed at 30°C for 3,12, 24 and 48 hours. α-tubulin or GAPDH was used as loading control. (n=6-8 biologically independent samples/group) Comparisons are made with one-way ANOVA with post hoc Tukey's test; data are presented as mean ± SD. *$p<0.05$.

4 Discussion

The present study demonstrates the alterations in whole-body bioenergetics and changes in BAT metabolism *in-vivo* during 48 hours of cold-deacclimation. Our research demonstrates that BAT mitochondrial capacity decreases during the 24–48-hour period of cold-deacclimation. It is also important to note that although there was no discernible change in the overall UCP1 protein amount, there was a significant reduction in the total complex I and II proteins in iBAT. This decline could be attributed to an increase in mitophagy, confirmed by a decrease in total protein content and consistent with alterations in mitochondria and cristae ultrastructure.

BAT is key to whole body thermoregulation, particularly in small mammals and in infancy in humans[263–265]. To thermoregulate and adapt to cold environments, BAT generates heat by uncoupling respiration. Several substrates can be oxidized to generate heat in BAT during thermogenesis. Quantifying the RER during cold exposure can determine if fats or carbohydrates were consumed as energy substrates at the whole body level[266–269]. Previous studies have observed that intermittent cold exposure (4°C for 3h for day and 6 h for 8-10 days) increased energy expenditure and RER during light phase in mice[270]. Similarly, energy expenditure was found to increase when mice were moved from 33°C to 8°C[271]. Our study revealed that real-time whole-body oxygen consumption decreases within 3-120 hours of cold-deacclimation. This implies that the body's energy requirements and metabolic rate are reduced immediately upon cold-deacclimation. The shift in the metabolic profile was evident from the increased RER values at 12 hours of cold-deacclimation from our results. Thus, our results provide insights about the changes in whole-body metabolism during cold-deacclimation.

As oxidative capacity and metabolism are closely linked, we also determined effects of cold-deacclimation on BAT mitochondrial function. A study in humans indicated a 2.2 fold increase in the oxidative capacity of BAT during cold exposure (4°C for 4 weeks) to contribute to increase in NST[131]. The metabolic capacity of BAT can be altered by changes in blood flow or in nutrient availability during cold-deacclimation. Our results showed a decline in complex I, II, and cGPDH leaks at T3-T48 in tissue aliquots. However, isolated BAT mitochondria showed a decrease in Complex II and cGPDG-mediated respiration at T48 compared to T0. The isolated BAT mitochondria might be resilient to the changes in temperature for up to 24 hours; nevertheless, a decrease in its capacity was apparent at 48 hours. This decrease in mitochondrial respiration could be related to the loss of damaged mitochondria in the isolation process. Our

study also pointed a decrease in the capacity of complex II mediated respiration in BAT during cold-deacclimation.

Moreover, a recent study revealed that on inducing low membrane potential in BAT mitochondria akin to the conditions experienced during cold exposure, RET decreased and oxaloacetate accumulated[272]. This accumulation of oxaloacetate decreases complex II respiration in BAT mitochondria[272]. Thus, future research should elucidate the acute changes in complex II activity and membrane potential upon cold-deacclimation.

Cold exposure increases BAT vascularity, cellularity, mitochondrial content, and metabolic rate [270, 273, 274]. BAT is highly flexible with remarkable tissue plasticity, as demonstrated by alterantions in metabolic rate, mitochondrial content decreases with increase in lipid content[228]. Our findings demonstrate a reduction in overall protein, mitochondrial content, and mitochondrial area during cold-deacclimation. Our observation is consistent with previous studies, where a decrease in protein content was noted during cold-deacclimation[228, 275]. UCP1 is the most abundant protein in BAT mitochondria whose expression increases about 5-fold on cold exposure[59]. However, studies have indicated a decrease in UCP1 mRNA expression after one day of cold-deacclimation[228]. Surprisingly, no change was observed in the UCP1 levels in iBAT while shifting mice from cold to thermoneutrality for 48 hours. However, the 48h time point may have not been long enough to detect changes in UCP1, as UCP1 has a long half-life (20-100 h), indicating its expression remains unchanged for a long time[255, 276, 277]. In contrast, the protein levels of complex I, II and III in iBAT after 48 h of cold-deacclimation, which is in line with previous findings that protein levels of complex II, IV and V can decrease after 1 day of cold-deacclimation[228].This decrease in OXPHOS proteins likely contributes to the decrease in BAT oxidative capacity during cold-deacclimation. Thus, the mitochondrial content and respiratory capacity of BAT decrease upon cold- deacclimation.

TEM is a sensitive technique that helps to determine the changes in mitochondria ultrastructure and detect structures like autophagosomes[278]. A qualitative study reported the presence of double-membrane autophagosomes and the presence of mitochondria-derived vesicles (MDVs) that indicates mitochondrial degradation was noted during 24h of cold-deacclimation[228]. These past results indicate the presence of large, elongated mitochondria and numerous mitophagosome

during cold exposure[231]. Detecting autophagosomes by TEM images can be subjective, so our study used western blots and a reporter mito-QC mice to identify autophagy/mitophagy. We also used the unbiased mito-QC counter approach to quantify mitolysosomes in BAT to measure mitophagy[195, 279]. Interestingly, our study which was designed to measure mitophagy during 3-48h of cold-deacclimation revealed an elevation in mitophagy at 48h of cold-deacclimation.

The PINK/ Parkin pathway was shown to be an important regulator of autophagy during cold-deacclimation[228]. However, we did not detect changes in the protein expression of Parkin and LC3 throughout the 48 hours of cold-deacclimation. It is important to note that the markers of autophagy/mitophagy might be quickly degraded by proteasome with changes in the membrane potential[195, 280]. This might be the potential reason western blot did not detect any changes in the protein levels of these markers. Interestingly, the protein levels of FUNDC1 decreased at T48, indicating a decrease in mitophagy. Previous studies have indicated a role for FUNDC1 in the coordination of with fission or fusion to mediate Parkin-independent mitophagy[204, 281]. Interestingly studies have shown mTORC1 and AMPK to regulate autophagy markers including FUNDC1[213, 282]. Thus, there is a possibility that these regulators (i.e. mTORC1 and AMPK) or several post-translation modifications might modify the levels of FUNDC1 which should be further investigated. More generally, further research should examine the role of AMPK and mTORC1 in BAT during cold exposure and cold-deacclimation.

Our analyses of BAT using TEM showed that mitochondrial fragmentation and glycogen granules increased throughout the cold-deacclimation period. Our results also point towards decreased mitochondrial area and cristae volume which might also be an indication of increased mitophagy. While cold exposure induces BAT lipolysis[283, 228], triglycerides accumulate into larger lipid droplets at warm environmental temperatures[284–286], and this is associated with the upregulation of enzymes involved in fatty acid synthesis, such as fatty acid synthase[287]. Our findings of increased lipid droplet number and size in BAT during cold-deacclimation are in line with previous findings in rats[288].

Conclusions

Overall, our findings are consistent with the conclusion that increased mitophagy during cold-deacclimation partially contributes to decreased mitochondria size and content. Our findings are altogether in-keeping with our observations of decreased whole body energy expenditure and BAT mitochondria-specific oxygen consumption during cold-deacclimation. Apart from functional changes, cold-deacclimation decreases mitochondrial number and lipid number; increases lipid size, and is associated with changes in BAT mitochondrial ultrastructure. Overall, our findings advance the understanding of the fundamental mechanisms that 'turn off' BAT thermogenesis when it is not needed, thereby enhancing survival capacity of the animal.

Limitations

As we carried out cold-deacclimation studies in mice, and as mice thermoregulate differently than other mammals including humans, it is important to not overinterpret the findings for humans.

It has been reported that the Mito-QC counter can overestimate the number of mitolysosomes than anticipated as it does not take the dimension of the mitolysosomes into consideration[289]. Thus, it is important to consider this limitation in the interpretation of results.

Finally, while high resolution respirometry is useful in investigating mitochondrial respiration in *ex-vivo* and *in-vitro* samples, it measures mitochondrial capacity, and not the actual activity *in-vivo*.

Alternative approaches and future directions

To complement the assessments of mitophagy described in this thesis, additional determinations should include mitophagic flux analyses (i.e., LC3 turnover assay, live cell imaging or comparing autophagosome numbers in the absence and presence of lysosomal inhibitors.) to quantify the rate of mitophagy and to understand the dynamics of mitophagy in BAT during cold exposure and cold-deacclimation.

Moreover, mitochondrial lysates should be studied as well as cell lysates for western blot analysis. Mitochondrial lysates would allow us to detect differences in the presence and levels of key proteins involved in mitophagy and mitochondrial dynamics.

In the future it would be interesting to assess the *in-vivo* functional changes in BAT during cold-deacclimation. Approaches could include: ^{13}C-Glucose tracing using mass spectrometry, as well as 18F-Fluorodeoxyglucose- and 18F-Fluorothiaheptadecanoic acid- positron emission tomography (^{18}FDG-PET and ^{18}F-FTHA-PET, respectively).

5 References

1. Kahn, B. B. & Flier, J. S. Obesity and insulin resistance. *The Journal of clinical investigation* **106**, 473–81 (2000).

2. Kim, S. & Moustaid-Moussa, N. Secretory, Endocrine and Autocrine/Paracrine Function of the Adipocyte. *The Journal of Nutrition* **130**, 3110S-3115S (2000).

3. Vázquez-Vela, M. E. F., Torres, N. & Tovar, A. R. White Adipose Tissue as Endocrine Organ and Its Role in Obesity. *Archives of Medical Research* **39**, 715–728 (2008).

4. Cedikova, M. *et al.* Mitochondria in White, Brown, and Beige Adipocytes. *Stem Cells International* **2016**, 1–11 (2016).

5. Park, A. Distinction of white, beige and brown adipocytes derived from mesenchymal stem cells. *WJSC* **6**, 33 (2014).

6. Reddy, P., Lent-Schochet, D., Ramakrishnan, N., McLaughlin, M. & Jialal, I. Metabolic syndrome is an inflammatory disorder: A conspiracy between adipose tissue and phagocytes. *Clinica Chimica Acta* **496**, 35–44 (2019).

7. Chait, A. & Den Hartigh, L. J. Adipose Tissue Distribution, Inflammation and Its Metabolic Consequences, Including Diabetes and Cardiovascular Disease. *Front. Cardiovasc. Med.* **7**, 22 (2020).

8. Klein, S. *et al.* Waist Circumference and Cardiometabolic Risk. *Diabetes Care* **30**, 1647–1652 (2007).

9. Foster, M. T. & Pagliassotti, M. J. Metabolic alterations following visceral fat removal and expansion: Beyond anatomic location. *Adipocyte* **1**, 192–199 (2012).

10. W, F. Archiv für mikroskopische Anatomie, Band. *Anatomie* **7**, 357–367 (1871).

11. Ottaviani, E., Malagoli, D. & Franceschi, C. The evolution of the adipose tissue: a neglected enigma. *General and comparative endocrinology* **174**, 1–4 (2011).

12. Fonseca-Alaniz, M. H., Takada, J., Alonso-Vale, M. I. C. & Lima, F. B. O tecido adiposo como centro regulador do metabolismo. *Arquivos Brasileiros de Endocrinologia & Metabologia* **50**, 216–229 (2006).
13. Hadi, H. E., Vincenzo, A. D., Vettor, R. & Rossato, M. Food Ingredients Involved in White-to-Brown Adipose Tissue Conversion and in Calorie Burning. *Frontiers in physiology* **9**, 1954 (2018).
14. Kopecký, J. *et al.* Energy metabolism of adipose tissue–physiological aspects and target in obesity treatment. *Physiological research* **53 Suppl 1**, S225-32 (2004).
15. Böttcher, H. & Fürst, P. Decreased white fat cell thermogenesis in obese individuals. *Int J Obes* **21**, 439–444 (1997).
16. Schweiger, M. *et al.* Adipose Triglyceride Lipase and Hormone-sensitive Lipase Are the Major Enzymes in Adipose Tissue Triacylglycerol Catabolism. *Journal of Biological Chemistry* **281**, 40236–40241 (2006).
17. Coelho, M., Oliveira, T. & Fernandes, R. State of the art paper Biochemistry of adipose tissue: an endocrine organ. *Archives of Medical Science* **2**, 191–200 (2013).
18. Ahima, R. S. & Flier, J. S. Adipose Tissue as an Endocrine Organ. *Trends in Endocrinology & Metabolism* **11**, 327–332 (2000).
19. Saely, C. H., Geiger, K. & Drexel, H. Brown versus White Adipose Tissue: A Mini-Review. *Gerontology* **58**, 15–23 (2012).
20. Fonseca-Alaniz, M. H., Takada, J., Alonso-Vale, M. I. C. & Lima, F. B. Adipose tissue as an endocrine organ: from theory to practice. *Jornal de Pediatria* **10**, 987 (2007).
21. Bernlohr, D. A., Jenkins, A. E. & Bennaars, A. A. Chapter 10 Adipose tissue and lipid metabolism. in 263–289 (2002). doi:10.1016/S0167-7306(02)36012-5.

22. Christiaens, V. & Lijnen, H. R. Angiogenesis and development of adipose tissue. *Molecular and cellular endocrinology* **318**, 2–9 (2010).
23. Fischer-Posovszky, P. & Möller, P. Das Fettgewebe im Fokus des Immunsystems: adipositasassoziierte Inflammation. *Der Pathologe* **41**, 224–229 (2020).
24. Mathew, H., Castracane, V. D. & Mantzoros, C. Adipose tissue and reproductive health. *Metabolism* **86**, 18–32 (2018).
25. Pilkington, A.-C., Paz, H. A. & Wankhade, U. D. Beige Adipose Tissue Identification and Marker Specificity—Overview. *Frontiers in Endocrinology* **12**, 578 (2021).
26. Heim, T. & Hull, D. The blood flow and oxygen consumption of brown adipose tissue in the new-born rabbit. *The Journal of Physiology* **186**, 42–55 (1966).
27. Cypess, A. M. *et al.* Identification and Importance of Brown Adipose Tissue in Adult Humans. *New England Journal of Medicine* **360**, 1509–1517 (2009).
28. Orava, J. *et al.* Different Metabolic Responses of Human Brown Adipose Tissue to Activation by Cold and Insulin. *Cell Metabolism* **14**,567 (2011).
29. Lichtenbelt, W. D. van M. *et al.* Cold-Activated Brown Adipose Tissue in Healthy Men. *New England Journal of Medicine* **360**, 1500–1508 (2009).
30. Muzik, O. *et al.* ^{15} O PET Measurement of Blood Flow and Oxygen Consumption in Cold-Activated Human Brown Fat. *J Nucl Med* **54**, 523–531 (2013).
31. Carpentier, A. C. *et al.* Brown Adipose Tissue Energy Metabolism in Humans. *Frontiers in Endocrinology* **9**, 678 (2018).
32. Virtanen, K. A. *et al.* Functional Brown Adipose Tissue in Healthy Adults. *New England Journal of Medicine* **360**, 1518–1525 (2009).

33. Marlatt, K. L. & Ravussin, E. Brown Adipose Tissue: an Update on Recent Findings. *Current Obesity Reports* **6**, 389–396 (2017).

34. Hany, T. F. *et al.* Brown adipose tissue: a factor to consider in symmetrical tracer uptake in the neck and upper chest region. *European Journal of Nuclear Medicine and Molecular Imaging* **29**, 1393–1398 (2002).

35. Heaton, J. M. The distribution of brown adipose tissue in the human. *J. Anat.* **112**, 35–39 (1972).

36. Zhang, F. *et al.* An Adipose Tissue Atlas: An Image-Guided Identification of Human-like BAT and Beige Depots in Rodents. *Cell Metabolism* **27**, 252-262.e3 (2018).

37. Nedergaard, J., Bengtsson, T. & Cannon, B. Unexpected evidence for active brown adipose tissue in adult humans. *American Journal of Physiology-Endocrinology and Metabolism* **293**, E444–E452 (2007).

38. Ouellet, V. *et al.* Brown adipose tissue oxidative metabolism contributes to energy expenditure during acute cold exposure in humans. *Journal of Clinical Investigation* **122**, 234(2012).

39. Lidell, M. E. *et al.* Evidence for two types of brown adipose tissue in humans. *Nature Medicine* **19**, 631–634 (2013).

40. Mo, Q. *et al.* Identification and characterization of a supraclavicular brown adipose tissue in mice. *JCI insight* **2**,167 (2017).

41. Sidossis, L. & Kajimura, S. Brown and beige fat in humans: thermogenic adipocytes that control energy and glucose homeostasis. *Journal of Clinical Investigation* **125**, 478–486 (2015).

42. Bal, N. C. *et al.* Sarcolipin is a newly identified regulator of muscle-based thermogenesis in mammals. *Nat Med* **18**, 1575–1579 (2012).

43. Smith, R. E. & Roberts, J. C. Thermogenesis of brown adipose tissue in cold-acclimated rats. *American Journal of Physiology-Legacy Content* **206**, 143–148 (1964).
44. Oelkrug, R., Polymeropoulos, E. T. & Jastroch, M. Brown adipose tissue: physiological function and evolutionary significance. *J Comp Physiol B* **185**, 587–606 (2015).
45. Yoneshiro, T. *et al.* Age-Related Decrease in Cold-Activated Brown Adipose Tissue and Accumulation of Body Fat in Healthy Humans. *Obesity* **19**, 1755–1760 (2011).
46. Dinas, P. C. *et al.* Association between habitual physical activity and brown adipose tissue activity in individuals undergoing PET-CT scan. *Clin Endocrinol* **82**, 147–154 (2015).
47. Cypess, A. M. & Kahn, C. R. The role and importance of brown adipose tissue in energy homeostasis. *Current Opinion in Pediatrics* **22**, 478–484 (2010).
48. Gaudry, M. J. & Jastroch, M. Hotly awaited structures obtained for the human protein UCP1. *Nature* **620**, 42–43 (2023).
49. Rosen, E. D. & Spiegelman, B. M. Adipocytes as regulators of energy balance and glucose homeostasis. *Nature* **444**, 847–853 (2006).
50. Frontini, A. & Cinti, S. Distribution and Development of Brown Adipocytes in the Murine and Human Adipose Organ. *Cell Metabolism* **11**, 253–256 (2010).
51. Li, L., Li, B., Li, M. & Speakman, J. R. Switching on the furnace: Regulation of heat production in brown adipose tissue. *Molecular Aspects of Medicine* **68**,145 (2019).
52. Mitchell, P. Coupling of Phosphorylation to Electron and Hydrogen Transfer by a Chemi-Osmotic type of Mechanism. *Nature* **191**, 144–148 (1961).
53. Divakaruni, A. S. & Brand, M. D. The Regulation and Physiology of Mitochondrial Proton Leak. *Physiology* **26**, 192–205 (2011).

54. Busiello, R. A., Savarese, S. & Lombardi, A. Mitochondrial uncoupling proteins and energy metabolism. *Frontiers in Physiology* **6**,123 (2015).

55. Gesta, S., Tseng, Y.-H. & Kahn, C. R. Developmental Origin of Fat: Tracking Obesity to Its Source. *Cell* **131**, 242–256 (2007).

56. Cannon, B. & Nedergaard, J. Brown Adipose Tissue: Function and Physiological Significance. *Physiological Reviews* **84**, 124 (2004).

57. Heaton, G. M., Wagenvoord, R. J., Kemp, A. & Nicholls, D. G. Brown-Adipose-Tissue Mitochondria: Photoaffinity Labelling of the Regulatory Site of Energy Dissipation. *Eur J Biochem* **82**, 515–521 (1978).

58. Krauss, S., Zhang, C.-Y. & Lowell, B. B. The mitochondrial uncoupling-protein homologues. *Nature Reviews Molecular Cell Biology* **6**, 99(2005).

59. Nedergaard, J. & Cannon, B. UCP1 mRNA does not produce heat. *Biochimica et Biophysica Acta (BBA) - Molecular and Cell Biology of Lipids* **1831**, 943–949 (2013).

60. Pebay-Peyroula, E. *et al.* Structure of mitochondrial ADP/ATP carrier in complex with carboxyatractyloside. *Nature* **426**, 39–44 (2003).

61. Fedorenko, A., Lishko, P. V. & Kirichok, Y. Mechanism of Fatty-Acid-Dependent UCP1 Uncoupling in Brown Fat Mitochondria. *Cell* **151**,122 (2012).

62. Chang, S.-H. *et al.* Nrf2 induces Ucp1 expression in adipocytes in response to β3-AR stimulation and enhances oxygen consumption in high-fat diet-fed obese mice. *BMB Rep* **54**, 419–424 (2021).

63. Dempersmier, J. *et al.* Cold-Inducible Zfp516 Activates UCP1 Transcription to Promote Browning of White Fat and Development of Brown Fat. *Molecular Cell* **57**, 235–246 (2015).

64. Chouchani, E. T. *et al.* Mitochondrial ROS regulate thermogenic energy expenditure and sulfenylation of UCP1. *Nature* **532**, 112 (2016).

65. Rial, E., Poustie, A. & Nicholls, D. G. Brown-adipose-tissue mitochondria: the regulation of the 32 000-Mr uncoupling protein by fatty acids and purine nucleotides. *European Journal of Biochemistry* **137**, 197–203 (1983).

66. Modrianský, M., Murdza-Inglis, D. L., Patel, H. V., Freeman, K. B. & Garlid, K. D. Identification by Site-directed Mutagenesis of Three Arginines in Uncoupling Protein That Are Essential for Nucleotide Binding and Inhibition. *Journal of Biological Chemistry* **272**, 24759–24762 (1997).

67. Klingenberg, M. Wanderings in bioenergetics and biomembranes. *Biochimica et Biophysica Acta (BBA) - Bioenergetics* **1797**, 579–594 (2010).

68. Breen, E. P. *et al.* On the Mechanism of Mitochondrial Uncoupling Protein 1 Function. *Journal of Biological Chemistry* **281**, 2114–2119 (2006).

69. Shabalina, I. G., Jacobsson, A., Cannon, B. & Nedergaard, J. Native UCP1 Displays Simple Competitive Kinetics between the Regulators Purine Nucleotides and Fatty Acids. *Journal of Biological Chemistry* **279**,34 (2004).

70. Winkler, E. & Klingenberg, M. Effect of fatty acids on H+ transport activity of the reconstituted uncoupling protein. *The Journal of biological chemistry* **269**, 2508–15 (1994).

71. Garlid, K. D., Jabůrek, M. & Ježek, P. The mechanism of proton transport mediated by mitochondrial uncoupling proteins. *FEBS Letters* **438**, 10–14 (1998).

72. Klingenberg, M. & Winkler, E. The reconstituted isolated uncoupling protein is a membrane potential driven H+ translocator. *The EMBO Journal* **4**, 3087–3092 (1985).

73. Nicholls, D. G. The physiological regulation of uncoupling proteins. *Biochimica et Biophysica Acta (BBA) - Bioenergetics* **1757**,1234 (2006).

74. Sluse, F. E. *et al.* Mitochondrial UCPs: new insights into regulation and impact. *Biochimica et biophysica acta* **1757**, 480–5 (2006).

75. Lehr, L. *et al.* The control of UCP1 is dissociated from that of PGC-1alpha or of mitochondriogenesis as revealed by a study using beta-less mouse brown adipocytes in culture. *FEBS letters* **580**, 4661–6 (2006).

76. Takahashi, Y. & Ide, T. Dietary *n* -3 fatty acids affect mRNA level of brown adipose tissue uncoupling protein 1, and white adipose tissue leptin and glucose transporter 4 in the rat. *Br J Nutr* **84**, 175–184 (2000).

77. You, M., Fan, R., Kim, J., Shin, S.-H. & Chung, S. Alpha-Linolenic Acid-Enriched Butter Promotes Fatty Acid Remodeling and Thermogenic Activation in the Brown Adipose Tissue. *Nutrients* **12**, 136 (2020).

78. Bargut, T. C. L., Silva-e-Silva, A. C. A. G., Souza-Mello, V., Mandarim-de-Lacerda, C. A. & Aguila, M. B. Mice fed fish oil diet and upregulation of brown adipose tissue thermogenic markers. *Eur J Nutr* **55**, 159–169 (2016).

79. Nicholls, D. G. & Locke, R. M. Thermogenic mechanisms in brown fat. *Physiological Reviews* **64**, 1–64 (1984).

80. Cannon, B. & Nedergaard, J. The biochemistry of an inefficient tissue: brown adipose tissue. *Essays in biochemistry* **20**, 234-245 (1985).

81. Enerbäck, S. *et al.* Mice lacking mitochondrial uncoupling protein are cold-sensitive but not obese. *Nature* **387**, 90–94 (1997).

82. Brand, M. D. & Esteves, T. C. Physiological functions of the mitochondrial uncoupling proteins UCP2 and UCP3. *Cell Metabolism* **2**, 85–93 (2005).

83. Zhao, R., Jiang, S., Zhang, L. & Yu, Z. Mitochondrial electron transport chain, ROS generation and uncoupling (Review). *Int J Mol Med* 1032 (2019) doi:10.3892/ijmm.2019.4188.

84. Ricquier, D. & Bouillaud, F. The uncoupling protein homologues: UCP1, UCP2, UCP3, StUCP and AtUCP. *Biochemical Journal* **345**, 161–179 (2000).

85. Pohl, E. E., Rupprecht, A., Macher, G. & Hilse, K. E. Important Trends in UCP3 Investigation. *Frontiers in Physiology* **10**,102-120 (2019).

86. Silvestri, E. *et al.* Absence of uncoupling protein 3 at thermoneutrality influences brown adipose tissue mitochondrial functionality in mice. *The FASEB Journal* **34**, 15146–15163 (2020).

87. Sacks, H. & Symonds, M. E. Anatomical Locations of Human Brown Adipose Tissue. *Diabetes* **62**, 1783–1790 (2013).

88. Inagaki, T., Sakai, J. & Kajimura, S. Erratum: Transcriptional and epigenetic control of brown and beige adipose cell fate and function. *Nature Reviews Molecular Cell Biology* **18**, 527–527 (2017).

89. Barbatelli, G. *et al.* The emergence of cold-induced brown adipocytes in mouse white fat depots is determined predominantly by white to brown adipocyte transdifferentiation. *American journal of physiology. Endocrinology and metabolism* **298**, E1244-53 (2010).

90. Chang, L., Garcia-Barrio, M. T. & Chen, Y. E. Perivascular Adipose Tissue Regulates Vascular Function by Targeting Vascular Smooth Muscle Cells. *Arteriosclerosis, Thrombosis, and Vascular Biology* **40**, 1094–1109 (2020).

91. Gaborit, B. *et al.* Human epicardial adipose tissue has a specific transcriptomic signature depending on its anatomical peri-atrial, peri-ventricular, or peri-coronary location. *Cardiovascular Research* **108**, 62–73 (2015).
92. Sacks, H. S. *et al.* Adult Epicardial Fat Exhibits Beige Features. *The Journal of Clinical Endocrinology & Metabolism* **98**, E1448–E1455 (2013).
93. Seale, P. *et al.* Prdm16 determines the thermogenic program of subcutaneous white adipose tissue in mice. *Journal of Clinical Investigation* **121**, 96–105 (2011).
94. Cousin, B. *et al.* Adipose tissues from various anatomical sites are characterized by different patterns of gene expression and regulation. *Biochemical Journal* **292**,101-120 (1993).
95. Collins, S., Daniel, K. W., Petro, A. E. & Surwit, R. S. Strain-Specific Response toβ_3-Adrenergic Receptor Agonist Treatment of Diet-Induced Obesity in Mice [1]. *Endocrinology* **138**,1234 (1997).
96. Cousin, B. *et al.* Occurrence of brown adipocytes in rat white adipose tissue: molecular and morphological characterization. *Journal of Cell Science* **103**, 931–942 (1992).
97. Guerra, C., Koza, R. A., Yamashita, H., Walsh, K. & Kozak, L. P. Emergence of brown adipocytes in white fat in mice is under genetic control. Effects on body weight and adiposity. *J. Clin. Invest.* **102**, 412–420 (1998).
98. Ghorbani, M. & Himms-Hagen, J. Appearance of brown adipocytes in white adipose tissue during CL 316,243-induced reversal of obesity and diabetes in Zucker fa/fa rats. *International journal of obesity and related metabolic disorders : journal of the International Association for the Study of Obesity* **21**, 465–75 (1997).
99. Young, P., Arch, J. R. S. & Ashwell, M. Brown adipose tissue in the parametrial fat pad of the mouse. *FEBS Letters* **167**, 10–14 (1984).

100. Azhar, Y., Parmar, A., Miller, C. N., Samuels, J. S. & Rayalam, S. Phytochemicals as novel agents for the induction of browning in white adipose tissue. *Nutrition & Metabolism* **13**, 89 (2016).

101. Mössenböck, K. *et al.* Browning of White Adipose Tissue Uncouples Glucose Uptake from Insulin Signaling. *PLoS ONE* **9**, e110428 (2014).

102. Pereira, R. O. *et al.* OPA1 Regulates Lipid Metabolism and Cold-Induced Browning of White Adipose Tissue in Mice. *Diabetes* **71**, 2572–2583 (2022).

103. Morton, G. J. Hypothalamic leptin regulation of energy homeostasis and glucose metabolism. *The Journal of Physiology* **583**, 437–443 (2007).

104. Morrison, S. F. & Nakamura, K. Central Mechanisms for Thermoregulation. *Annu. Rev. Physiol.* **81**, 285–308 (2019).

105. Tan, C. L. & Knight, Z. A. Regulation of Body Temperature by the Nervous System. *Neuron* **98**, 31–48 (2018).

106. Veicsteinas, A., Ferretti, G. & Rennie, D. W. Superficial shell insulation in resting and exercising men in cold water. *Journal of Applied Physiology* **52**, 1557–1564 (1982).

107. Zhao, J., Cannon, B. & Nedergaard, J. Thermogenesis is beta3- but not beta1-adrenergically mediated in rat brown fat cells, even after cold acclimation. *The American journal of physiology* **275**, R2002-11 (1998).

108. Bronnikov, G. *et al.* beta1 to beta3 switch in control of cyclic adenosine monophosphate during brown adipocyte development explains distinct beta-adrenoceptor subtype mediation of proliferation and differentiation. *Endocrinology* **140**, 4185–97 (1999).

109. Bachman, E. S. *et al.* βAR Signaling Required for Diet-Induced Thermogenesis and Obesity Resistance. *Science* **297**, 843–845 (2002).

110. MD, B. B. L., PhD & MD, J. S. F. Brown adipose tissue, β3-adrenergic receptors, and obesity. *Annual Review of Medicine* **48**, 307–316 (1997).

111. Reverte-Salisa, L., Sanyal, A. & Pfeifer, A. Role of cAMP and cGMP Signaling in Brown Fat. in 161–182 (2018). doi:10.1007/164_2018_117.

112. Cao, W. *et al.* p38 Mitogen-Activated Protein Kinase Is the Central Regulator of Cyclic AMP-Dependent Transcription of the Brown Fat Uncoupling Protein 1 Gene. *Molecular and Cellular Biology* **24**, 3057–3067 (2004).

113. Liang, H. & Ward, W. F. PGC-1α: a key regulator of energy metabolism. *Advances in Physiology Education* **30**, 145–151 (2006).

114. Miyoshi, H. *et al.* Control of Adipose Triglyceride Lipase Action by Serine 517 of Perilipin A Globally Regulates Protein Kinase A-stimulated Lipolysis in Adipocytes. *Journal of Biological Chemistry* **282**, 996–1002 (2007).

115. Jenkins, C. M. *et al.* Identification, Cloning, Expression, and Purification of Three Novel Human Calcium-independent Phospholipase A2 Family Members Possessing Triacylglycerol Lipase and Acylglycerol Transacylase Activities. *Journal of Biological Chemistry* **279**, 48968–48975 (2004).

116. Villena, J. A., Roy, S., Sarkadi-Nagy, E., Kim, K.-H. & Sul, H. S. Desnutrin, an Adipocyte Gene Encoding a Novel Patatin Domain-containing Protein, Is Induced by Fasting and Glucocorticoids. *Journal of Biological Chemistry* **279**, 47066–47075 (2004).

117. Zimmermann, R. *et al.* Fat Mobilization in Adipose Tissue Is Promoted by Adipose Triglyceride Lipase. *Science* **306**, 1383–1386 (2004).

118. Cao, W., Medvedev, A. V., Daniel, K. W. & Collins, S. β-Adrenergic Activation of p38 MAP Kinase in Adipocytes. *Journal of Biological Chemistry* **276**, 27077–27082 (2001).

119. Dickson, L. M., Gandhi, S., Layden, B. T., Cohen, R. N. & Wicksteed, B. Protein kinase A induces UCP1 expression in specific adipose depots to increase energy expenditure and improve metabolic health. *American Journal of Physiology-Regulatory, Integrative and Comparative Physiology* **311**, R79–R88 (2016).

120. Robidoux, J. *et al.* Selective Activation of Mitogen-Activated Protein (MAP) Kinase Kinase 3 and p38α MAP Kinase Is Essential for Cyclic AMP-Dependent UCP1 Expression in Adipocytes. *Molecular and Cellular Biology* **25**, 5466–5479 (2005).

121. Sears, I. B., MacGinnitie, M. A., Kovacs, L. G. & Graves, R. A. Differentiation-Dependent Expression of the Brown Adipocyte Uncoupling Protein Gene: Regulation by Peroxisome Proliferator-Activated Receptor γ. *Molecular and Cellular Biology* **16**, 3410–3419 (1996).

122. Kozak, U. C. *et al.* An upstream enhancer regulating brown-fat-specific expression of the mitochondrial uncoupling protein gene. *Molecular and Cellular Biology* **14**, 59–67 (1994).

123. Yubero, P. *et al.* Dominant Negative Regulation by c-Jun of Transcription of the Uncoupling Protein-1 Gene through a Proximal cAMP-Regulatory Element: A Mechanism for Repressing Basal and Norepinephrine-Induced Expression of the Gene before Brown Adipocyte Differentiation. *Molecular Endocrinology* **12**, 1023–1037 (1998).

124. Heldmaier, G. Temperature adaptation and brown adipose tissue in hairless and albino mice. *Journal of Comparative Physiology* **92**, 281–292 (1974).

125. Baba, S., Engles, J. M., Huso, D. L., Ishimori, T. & Wahl, R. L. Comparison of Uptake of Multiple Clinical Radiotracers into Brown Adipose Tissue Under Cold-Stimulated and Nonstimulated Conditions. *Journal of Nuclear Medicine* **48**, 1715–1723 (2007).

126. Giordano, A. *et al.* Sensory nerves affect the recruitment and differentiation of rat periovarian brown adipocytes during cold acclimation. *Journal of cell science* **111 (Pt 17)**, 2587–94 (1998).

127. Klingenspor, M. Cold-Induced Recruitment of Brown Adipose Tissue Thermogenesis. *Experimental Physiology* **88**, 141–148 (2003).

128. Lowell, B. B. & Spiegelman, B. M. Towards a molecular understanding of adaptive thermogenesis. *Nature* **404**, 652–660 (2000).

129. Gordon, C. J. Thermal physiology of laboratory mice: Defining thermoneutrality. *Journal of Thermal Biology* **37**, 654–685 (2012).

130. Blondin, D. P. *et al.* Four-week cold acclimation in adult humans shifts uncoupling thermogenesis from skeletal muscles to brown adipose tissue. *The Journal of Physiology* **595**, 1234(2017).

131. Blondin, D. P. *et al.* Increased Brown Adipose Tissue Oxidative Capacity in Cold-Acclimated Humans. *The Journal of Clinical Endocrinology & Metabolism* **99**, (2014).

132. Wang, Z. *et al.* Chronic cold exposure enhances glucose oxidation in brown adipose tissue. *EMBO reports* **21**, 1121(2020).

133. Hao, Q. *et al.* Transcriptome profiling of brown adipose tissue during cold exposure reveals extensive regulation of glucose metabolism. *American Journal of Physiology-Endocrinology and Metabolism* **308**, E380–E392 (2015).

134. Shore, A. M. *et al.* Cold-Induced Changes in Gene Expression in Brown Adipose Tissue, White Adipose Tissue and Liver. *PLoS ONE* **8**, e68933 (2013).

135. Ricquier, D., Mory, G. & Hemon, P. Changes induced by cold adaptation in the brown adipose tissue from several species of rodents, with special reference to the mitochondrial components. *Canadian Journal of Biochemistry* **57**, 1262–1266 (1979).

136. Leone, T. C. *et al.* PGC-1alpha deficiency causes multi-system energy metabolic derangements: muscle dysfunction, abnormal weight control and hepatic steatosis. *PLoS biology* **3**, e101 (2005).

137. Lelliott, C. J. *et al.* Ablation of PGC-1β Results in Defective Mitochondrial Activity, Thermogenesis, Hepatic Function, and Cardiac Performance. *PLoS Biology* **4**, e369 (2006).

138. Wu, Z. *et al.* Mechanisms Controlling Mitochondrial Biogenesis and Respiration through the Thermogenic Coactivator PGC-1. *Cell* **98**, 115–124 (1999).

139. Scarpulla, R. C. Nuclear activators and coactivators in mammalian mitochondrial biogenesis. *Biochimica et Biophysica Acta (BBA) - Gene Structure and Expression* **1576**, 1–14 (2002).

140. Scarpulla, R. C. Transcriptional activators and coactivators in the nuclear control of mitochondrial function in mammalian cells. *Gene* **286**, 81–89 (2002).

141. Dillon, L. M., Rebelo, A. P. & Moraes, C. T. The role of PGC-1 coactivators in aging skeletal muscle and heart. *IUBMB Life* **64**, 231–241 (2012).

142. Puigserver, P. *et al.* A Cold-Inducible Coactivator of Nuclear Receptors Linked to Adaptive Thermogenesis. *Cell* **92**, 829–839 (1998).

143. Barberá, M. J. *et al.* Peroxisome Proliferator-activated Receptor α Activates Transcription of the Brown Fat Uncoupling Protein-1 Gene. *Journal of Biological Chemistry* **276**, 1486–1493 (2001).

144. Guan, H.-P., Ishizuka, T., Chui, P. C., Lehrke, M. & Lazar, M. A. Corepressors selectively control the transcriptional activity of PPARγ in adipocytes. *Genes & Development* **19**, 453– 461 (2005).

145. Huss, J. M., Kopp, R. P. & Kelly, D. P. Peroxisome Proliferator-activated Receptor Coactivator-1α (PGC-1α) Coactivates the Cardiac-enriched Nuclear Receptors Estrogen-related Receptor-α and -γ. *Journal of Biological Chemistry* **277**, 40265–40274 (2002).

146. Puigserver, P. & Spiegelman, B. M. Peroxisome Proliferator-Activated Receptor-γ Coactivator 1α (PGC-1α): Transcriptional Coactivator and Metabolic Regulator. *Endocrine Reviews* **24**, 78–90 (2003).

147. Sonoda, J., Mehl, I. R., Chong, L.-W., Nofsinger, R. R. & Evans, R. M. PGC-1β controls mitochondrial metabolism to modulate circadian activity, adaptive thermogenesis, and hepatic steatosis. *Proceedings of the National Academy of Sciences* **104**, 5223–5228 (2007).

148. Shibata, H., Perusse, F., Vallerand, A. & Bukowiecki, L. J. Cold exposure reverses inhibitory effects of fasting on peripheral glucose uptake in rats. *American Journal of Physiology-Regulatory, Integrative and Comparative Physiology* **257**, (1989).

149. Townsend, K. L. & Tseng, Y.-H. Brown fat fuel utilization and thermogenesis. *Trends in endocrinology and metabolism: TEM* **25**, 168–77 (2014).

150. Moura, M. A. F. *et al.* Brown adipose tissue glyceroneogenesis is activated in rats exposed to cold. *Pflugers Archiv : European journal of physiology* **449**, 463–9 (2005).

151. Brito, M. N. *et al.* Brown adipose tissue triacylglycerol synthesis in rats adapted to a high- protein, carbohydrate-free diet. *The American journal of physiology* **276**, R1003-9 (1999).

152. Held, N. M. *et al.* Pyruvate dehydrogenase complex plays a central role in brown adipocyte energy expenditure and fuel utilization during short-term beta-adrenergic activation. *Sci Rep* **8**, 9562 (2018).

153. Isler, D., Hill, H. P. & Meier, M. K. Glucose metabolism in isolated brown adipocytes under β -adrenergic stimulation. Quantitative contribution of glucose to total thermogenesis. *Biochemical Journal* **245**, 789–793 (1987).

154. Saggerson, E. D., McAllister, T. W. J. & Baht, H. S. Lipogenesis in rat brown adipocytes. Effects of insulin and noradrenaline, contributions from glucose and lactate as precursors and comparisons with white adipocytes. *Biochemical Journal* **251**, 701–709 (1988).

155. Ma, S. W. Y. & Foster, D. O. Uptake of glucose and release of fatty acids and glycerol by rat brown adipose tissue *in vivo*. *Can. J. Physiol. Pharmacol.* **64**, 609–614 (1986).

156. James, D. E., Strube, M. & Muecdler, M. Molecular cloning and characterization of an insulin-regulatable glucose transporter. *Nature* **338**, 83–87 (1989).

157. Dallner, O. S., Chernogubova, E., Brolinson, K. A. & Bengtsson, T. β_3 -Adrenergic Receptors Stimulate Glucose Uptake in Brown Adipocytes by Two Mechanisms Independently of Glucose Transporter 4 Translocation. *Endocrinology* **147**, 5730–5739 (2006).

158. Chernogubova, E., Cannon, B. & Bengtsson, T. Norepinephrine Increases Glucose Transport in Brown Adipocytes via β_3 -Adrenoceptors through a cAMP, PKA, and PI3-Kinase-Dependent Pathway Stimulating Conventional and Novel PKCs. *Endocrinology* **145**, 269–280 (2004).

159. Liu, R. *et al.* PI3K/AKT pathway as a key link modulates the multidrug resistance of cancers. *Cell Death Dis* **11**, 797 (2020).

160. Zhu, W. *et al.* Dihydroartemisinin suppresses glycolysis of LNCaP cells by inhibiting PI3K/AKT pathway and downregulating HIF-1α expression. *Life Sciences* **233**, 116730 (2019).

161. Ersahin, T., Tuncbag, N. & Cetin-Atalay, R. The PI3K/AKT/mTOR interactive pathway. *Mol. BioSyst.* **11**, 1946–1954 (2015).

162. Nikami, H., Shimizu, Y., Endoh, D., Yano, H. & Saito, M. Cold exposure increases glucose utilization and glucose transporter expression in brown adipose tissue. *Biochemical and Biophysical Research Communications* **185**, 1078–1082 (1992).

163. Winther, S. *et al.* Restricting glycolysis impairs brown adipocyte glucose and oxygen consumption. *American Journal of Physiology-Endocrinology and Metabolism* **314**, E214–E223 (2018).

164. Lee, P. *et al.* Brown Adipose Tissue Exhibits a Glucose-Responsive Thermogenic Biorhythm in Humans. *Cell Metabolism* **23**, 602–609 (2016).

165. Silva, J. E. Thyroid Hormone Control of Thermogenesis and Energy Balance. *Thyroid* **5**, 481–492 (1995).

166. Bianco, A. C., Salvatore, D., Gereben, B., Berry, M. J. & Larsen, P. R. Biochemistry, Cellular and Molecular Biology, and Physiological Roles of the Iodothyronine Selenodeiodinases. *Endocrine Reviews* **23**, 38–89 (2002).

167. López, M. *et al.* Hypothalamic AMPK and fatty acid metabolism mediate thyroid regulation of energy balance. *Nature Medicine* **16**, 1001–1008 (2010).

168. Jesus, L. A. de *et al.* The type 2 iodothyronine deiodinase is essential for adaptive thermogenesis in brown adipose tissue. *The Journal of clinical investigation* **108**, 1379–85 (2001).

169. Christoffolete, M. A. *et al.* Mice with targeted disruption of the Dio2 gene have cold-induced overexpression of the uncoupling protein 1 gene but fail to increase brown adipose tissue lipogenesis and adaptive thermogenesis. *Diabetes* **53**, 577–84 (2004).

170. Nedergaard, J., Dicker, A. & Cannon, B. The interaction between thyroid and brown-fat thermogenesis. Central or peripheral effects? *Annals of the New York Academy of Sciences* **813**, 712–7 (1997).

171. Silva, J. E. & Larsen, P. R. Adrenergic activation of triiodothyronine production in brown adipose tissue. *Nature* **305**, 712–713 (1983).

172. Fernandez, J. A., Mampel, T., Villarroya, F. & Iglesias, R. Direct assessment of brown adipose tissue as a site of systemic tri-iodothyronine production in the rat. *Biochemical Journal* **243**, 281–284 (1987).

173. Villarroya, J., Cereijo, R. & Villarroya, F. An endocrine role for brown adipose tissue? *American journal of physiology. Endocrinology and metabolism* **305**, E567-72 (2013).

174. Cao, Y. Adipose tissue angiogenesis as a therapeutic target for obesity and metabolic diseases. *Nature Reviews Drug Discovery* **9**,134-142 (2010).

175. Xue, Y. *et al.* Hypoxia-Independent Angiogenesis in Adipose Tissues during Cold Acclimation. *Cell Metabolism* **9**,121-131 (2009).

176. Lim, S. *et al.* Cold-induced activation of brown adipose tissue and adipose angiogenesis in mice. *Nature Protocols* **7**, 606–615 (2012).

177. Bagchi, M. *et al.* Vascular endothelial growth factor is important for brown adipose tissue development and maintenance. *The FASEB Journal* **27**, 3257–3271 (2013).

178. Asano, A., Kimura, K. & Saito, M. Cold-Induced mRNA Expression of Angiogenic Factors in Rat Brown Adipose Tissue. *The Journal of Veterinary Medical Science* **61**, 403–409 (1999).

179. Luo, X. *et al.* Cold Exposure Differentially Stimulates Angiogenesis in BAT and WAT of Mice: Implication in Adrenergic Activation. *Cellular Physiology and Biochemistry* **42**, 974–986 (2017).

180. Sun, K. *et al.* Brown adipose tissue derived VEGF-A modulates cold tolerance and energy expenditure. *Molecular Metabolism* **3**, 474–483 (2014).

181. Asano, A., Morimatsu, M., Nikami, H., Yoshida, T. & Saito, M. Adrenergic activation of vascular endothelial growth factor mRNA expression in rat brown adipose tissue: implication in cold-induced angiogenesis. *The Biochemical journal* **328 (Pt 1)**, 179–83 (1997).

182. Ashrafi, G. & Schwarz, T. L. The pathways of mitophagy for quality control and clearance of mitochondria. *Cell Death & Differentiation* **20**, 31–42 (2013).

183. Jung, C. H., Ro, S.-H., Cao, J., Otto, N. M. & Kim, D.-H. mTOR regulation of autophagy. *FEBS Letters* **584**, 1287–1295 (2010).

184. Tamargo-Gómez, I. & Mariño, G. AMPK: Regulation of Metabolic Dynamics in the Context of Autophagy. *International Journal of Molecular Sciences* **19**, 3812 (2018).

185. Russell, R. C. *et al.* ULK1 induces autophagy by phosphorylating Beclin-1 and activating VPS34 lipid kinase. *Nature cell biology* **15**, 741–50 (2013).

186. Klionsky, D. J. *et al.* A comprehensive glossary of autophagy-related molecules and processes (2nd edition). *Autophagy* **7**, 1273–94 (2011).

187. Dikic, I. & Elazar, Z. Mechanism and medical implications of mammalian autophagy. *Nat Rev Mol Cell Biol* **19**, 349–364 (2018).

188. Nakatogawa, H., Ishii, J., Asai, E. & Ohsumi, Y. Atg4 recycles inappropriately lipidated Atg8 to promote autophagosome biogenesis. *Autophagy* **8**, 177–186 (2012).

189. Nakatogawa, H., Ichimura, Y. & Ohsumi, Y. Atg8, a Ubiquitin-like Protein Required for Autophagosome Formation, Mediates Membrane Tethering and Hemifusion. *Cell* **130**, 165–178 (2007).

190. Kabeya, Y. LC3, a mammalian homologue of yeast Apg8p, is localized in autophagosome membranes after processing. *The EMBO Journal* **19**, 5720–5728 (2000).

191. Pankiv, S. *et al.* p62/SQSTM1 Binds Directly to Atg8/LC3 to Facilitate Degradation of Ubiquitinated Protein Aggregates by Autophagy. *Journal of Biological Chemistry* **282**, 24131–24145 (2007).

192. Truban, D., Hou, X., Caulfield, T. R., Fiesel, F. C. & Springer, W. PINK1, Parkin, and Mitochondrial Quality Control: What can we Learn about Parkinson's Disease Pathobiology? *Journal of Parkinson's Disease* **7**, 13–29 (2017).

193. Sarraf, S. A. *et al.* Landscape of the PARKIN-dependent ubiquitylome in response to mitochondrial depolarization. *Nature* **496**, 372–376 (2013).

194. Moore, A. S. & Holzbaur, E. L. F. Dynamic recruitment and activation of ALS-associated TBK1 with its target optineurin are required for efficient mitophagy. *Proceedings of the National Academy of Sciences* **113**, 1123(2016).

195. Yamano, K. & Youle, R. J. PINK1 is degraded through the N-end rule pathway. *Autophagy* **9**, 1758–1769 (2013).

196. Greene, A. W. *et al.* Mitochondrial processing peptidase regulates PINK1 processing, import and Parkin recruitment. *EMBO reports* **13**, 378–385 (2012).

197. Jin, S. M. *et al.* Mitochondrial membrane potential regulates PINK1 import and proteolytic destabilization by PARL. *Journal of Cell Biology* **191**, 933–942 (2010).

198. Kondapalli, C. *et al.* PINK1 is activated by mitochondrial membrane potential depolarization and stimulates Parkin E3 ligase activity by phosphorylating Serine 65. *Open Biology* **2**, 120080 (2012).

199. Okatsu, K. *et al.* Phosphorylated ubiquitin chain is the genuine Parkin receptor. *Journal of Cell Biology* **209**, 111–128 (2015).

200. Weidberg, H., Shvets, E. & Elazar, Z. Biogenesis and Cargo Selectivity of Autophagosomes. *Annu. Rev. Biochem.* **80**, 125–156 (2011).

201. Feng, Y., He, D., Yao, Z. & Klionsky, D. J. The machinery of macroautophagy. *Cell Research* **24**, 24–41 (2014).

202. Wong, Y. C. & Holzbaur, E. L. F. Optineurin is an autophagy receptor for damaged mitochondria in parkin-mediated mitophagy that is disrupted by an ALS-linked mutation. *Proceedings of the National Academy of Sciences* **111**,1231 (2014).

203. Heo, J.-M., Ordureau, A., Paulo, J. A., Rinehart, J. & Harper, J. W. The PINK1-parkin Mitochondrial Ubiquitylation Pathway Drives a Program of OPTN/NDP52 Recruitment and TBK1 Activation to Promote Mitophagy. *Molecular Cell* **60**, 7–20 (2015).

204. Liu, L. *et al.* Mitochondrial outer-membrane protein FUNDC1 mediates hypoxia-induced mitophagy in mammalian cells. *Nature Cell Biology* **14**, 177–185 (2012).

205. Novak, I. *et al.* Nix is a selective autophagy receptor for mitochondrial clearance. *EMBO reports* **11**, 45–51 (2010).

206. Hanna, R. A. *et al.* Microtubule-associated Protein 1 Light Chain 3 (LC3) Interacts with Bnip3 Protein to Selectively Remove Endoplasmic Reticulum and Mitochondria via Autophagy. *Journal of Biological Chemistry* **287**, 19094–19104 (2012).

207. Vande Velde, C. *et al.* BNIP3 and Genetic Control of Necrosis-Like Cell Death through the Mitochondrial Permeability Transition Pore. *Molecular and Cellular Biology* **20**, 5454–5468 (2000).

208. Kubasiak, L. A., Hernandez, O. M., Bishopric, N. H. & Webster, K. A. Hypoxia and acidosis activate cardiac myocyte death through the Bcl-2 family protein BNIP3. *Proceedings of the National Academy of Sciences* **99**, 12825–12830 (2002).

209. Kubli, D. A., Ycaza, J. E. & Gustafsson, Å. B. Bnip3 mediates mitochondrial dysfunction and cell death through Bax and Bak. *Biochemical Journal* **405**, 407–415 (2007).

210. Kim, J.-Y., Cho, J.-J., Ha, J. & Park, J.-H. The Carboxy Terminal C-Tail of BNip3 Is Crucial in Induction of Mitochondrial Permeability Transition in Isolated Mitochondria. *Archives of Biochemistry and Biophysics* **398**, 147–152 (2002).

211. Diwan, A. *et al.* Unrestrained erythroblast development in Nix $^{-/-}$ mice reveals a mechanism for apoptotic modulation of erythropoiesis. *Proc. Natl. Acad. Sci. U.S.A.* **104**, 6794–6799 (2007).

212. Crompton, M. The mitochondrial permeability transition pore and its role in cell death. *The Biochemical journal* **341 (Pt 2)**, 233–49 (1999).

213. Liu, L. *et al.* Mitophagy receptor FUNDC1 is regulated by PGC-1α/NRF1 to fine tune mitochondrial homeostasis. *EMBO reports* **22**,1323 (2021).

214. Cho, Y. K. *et al.* STK3/STK4 signalling in adipocytes regulates mitophagy and energy expenditure. *Nature Metabolism* **3**, 428–441 (2021).

215. Li, Z. *et al.* Determination of mitophagy by electron microscope. in 103–110 (2021). doi:10.1016/bs.mcb.2020.10.015.

216. Novak, I. & Dikic, I. Autophagy receptors in developmental clearance of mitochondria. *Autophagy* **7**, 301–303 (2011).

217. Ma, K. *et al.* Dynamic PGAM5 multimers dephosphorylate BCL-xL or FUNDC1 to regulate mitochondrial and cellular fate. *Cell Death & Differentiation* **27**, 1036–1051 (2020).

218. Chen, G. *et al.* A Regulatory Signaling Loop Comprising the PGAM5 Phosphatase and CK2 Controls Receptor-Mediated Mitophagy. *Molecular Cell* **54**, 362–377 (2014).

219. Liu, L., Sakakibara, K., Chen, Q. & Okamoto, K. Receptor-mediated mitophagy in yeast and mammalian systems. *Cell Research* **24**, 787–795 (2014).

220. Chan, D. C. Fusion and Fission: Interlinked Processes Critical for Mitochondrial Health. *Annu. Rev. Genet.* **46**, 265–287 (2012).

221. Youle, R. J. & Van Der Bliek, A. M. Mitochondrial Fission, Fusion, and Stress. *Science* **337**, 1062–1065 (2012).

222. Fu, W., Liu, Y. & Yin, H. Mitochondrial Dynamics: Biogenesis, Fission, Fusion, and Mitophagy in the Regulation of Stem Cell Behaviors. *Stem Cells International* **2019**, 1–15 (2019).

223. Levine, B. & Klionsky, D. J. Development by Self-Digestion. *Developmental Cell* **6**, 463– 477 (2004).

224. Mizushima, N. Autophagy: process and function. *Genes & Development* **21**, 2861–2873 (2007).

225. Singh, R. *et al.* Autophagy regulates adipose mass and differentiation in mice. *J. Clin. Invest.* JCI39228 (2009) doi:10.1172/JCI39228.

226. Yau, W. W. *et al.* Chronic cold exposure induces autophagy to promote fatty acid oxidation, mitochondrial turnover, and thermogenesis in brown adipose tissue. *iScience* **24**, 102434 (2021).

227. Cairó, M. *et al.* Thermogenic activation represses autophagy in brown adipose tissue. *International Journal of Obesity* **40**, 1591–1599 (2016).

228. Cairó, M. *et al.* Parkin controls brown adipose tissue plasticity in response to adaptive thermogenesis. *EMBO reports* **20**, 123-101 (2019).

229. Gospodarska, E., Nowialis, P. & Kozak, L. P. Mitochondrial Turnover. *Journal of Biological Chemistry* **290**, 8243–8255 (2015).

230. Altshuler-Keylin, S. *et al.* Beige Adipocyte Maintenance Is Regulated by Autophagy-Induced Mitochondrial Clearance. *Cell Metabolism* **24**, 402–419 (2016).

231. Lu, Y. *et al.* Mitophagy is required for brown adipose tissue mitochondrial homeostasis during cold challenge. *Scientific Reports* **8**, 123-148 (2018).

232. Wikstrom, J. D. *et al.* Hormone-induced mitochondrial fission is utilized by brown adipocytes as an amplification pathway for energy expenditure. *The EMBO Journal* n/a-n/a (2014) doi:10.1002/embj.201385014.

233. Shen, M. *et al.* Multi defect detection and analysis of electron microscopy images with deep learning. *Computational Materials Science* **199**, 110576 (2021).

234. Williams, J. A., Zhao, K., Jin, S. & Ding, W.-X. New methods for monitoring mitochondrial biogenesis and mitophagy *in vitro* and *in vivo*. *Exp Biol Med (Maywood)* **242**, 781–787 (2017).

235. Bass, J. J. *et al.* An overview of technical considerations for Western blotting applications to physiological research. *Scandinavian Journal of Medicine & Science in Sports* **27**, 4–25 (2017).

236. Kurien, B. T. & Scofield, R. H. Other notable protein blotting methods: a brief review. *Methods Mol Biol* **1312**, 487–503 (2015).

237. Murphy, R. M. & Lamb, G. D. Important considerations for protein analyses using antibody based techniques: down-sizing Western blotting up-sizes outcomes. *J Physiol* **591**, 5823–5831 (2013).

238. Kim, P. K., Hailey, D. W., Mullen, R. T. & Lippincott-Schwartz, J. Ubiquitin signals autophagic degradation of cytosolic proteins and peroxisomes. *Proc Natl Acad Sci U S A* **105**, 20567–20574 (2008).

239. Dolman, N. J., Chambers, K. M., Mandavilli, B., Batchelor, R. H. & Janes, M. S. Tools and techniques to measure mitophagy using fluorescence microscopy. *Autophagy* **9**, 1653– 1662 (2013).

240. Frigault, M. M., Lacoste, J., Swift, J. L. & Brown, C. M. Live-cell microscopy – tips and tools. *Journal of Cell Science* **122**, 753–767 (2009).

241. Wagner, M. *et al.* Light Dose is a Limiting Factor to Maintain Cell Viability in Fluorescence Microscopy and Single Molecule Detection. *IJMS* **11**, 956–966 (2010).

242. Katayama, H., Kogure, T., Mizushima, N., Yoshimori, T. & Miyawaki, A. A Sensitive and Quantitative Technique for Detecting Autophagic Events Based on Lysosomal Delivery. *Chemistry & Biology* **18**, 1042–1052 (2011).

243. Sun, N. *et al.* Measuring In Vivo Mitophagy. *Molecular Cell* **60**, 685–696 (2015).

244. Liu, Y.-T. *et al.* Mt-Keima detects PINK1-PRKN mitophagy *in vivo* with greater sensitivity than mito-QC. *Autophagy* **17**, 3753–3762 (2021).

245. Laker, R. C. *et al.* A Novel MitoTimer Reporter Gene for Mitochondrial Content, Structure, Stress, and Damage in Vivo. *Journal of Biological Chemistry* **289**, 12005–12015 (2014).

246. Trudeau, K. M., Gottlieb, R. A. & Shirihai, O. S. Measurement of Mitochondrial Turnover and Life Cycle Using MitoTimer. in 21–38 (2014). doi:10.1016/B978-0-12-801415-8.00002- 3.

247. Ferree, A. W. *et al.* MitoTimer probe reveals the impact of autophagy, fusion, and motility on subcellular distribution of young and old mitochondrial protein and on relative mitochondrial protein age. *Autophagy* **9**, 1887–1896 (2013).

248. Hernandez, G. *et al.* MitoTimer. *Autophagy* **9**, 1852–1861 (2013).

249. McWilliams, T. G. *et al.* mito-QC illuminates mitophagy and mitochondrial architecture in vivo. *Journal of Cell Biology* **214**, 111-121(2016).

250. McWilliams, T. G. & Ganley, I. G. Investigating Mitophagy and Mitochondrial Morphology In Vivo Using mito-QC: A Comprehensive Guide. in 123-133 (2019). doi:10.1007/978-1-4939-8873-0_41.

251. Mauro-Lizcano, M. *et al.* New method to assess mitophagy flux by flow cytometry. *Autophagy* **11**, 833–843 (2015).

252. Steiner, G., Loveland, M. & Schonbaum, E. Effect of denervation on brown adipose tissue metabolism. *American Journal of Physiology-Legacy Content* **218**, 566–570 (1970).

253. Desautels, M., Dulos, R. A. & Mozaffari, B. Selective loss of uncoupling protein from mitochondria of surgically denervated brown adipose tissue of cold-acclimated mice. *Biochem. Cell Biol.* **64**, 1125–1134 (1986).

254. Desautels, M. & Himms-Hagen, J. Parallel regression of cold-induced changes in ultrastructure, composition, and properties of brown adipose tissue mitochondria during recovery of rats from acclimation to cold. *Can. J. Biochem.* **58**, 1057–1068 (1980).

255. Lipsky, N. G. & Pedersen, P. L. Mitochondrial turnover in animal cells. Half-lives of mitochondria and mitochondrial subfractions of rat liver based on [14C] bicarbonate incorporation. *Journal of Biological Chemistry* **256**, 8652–8657 (1981).

256. Riachi, M., Himms-Hagen, J. & Harper, M.-E. Percent relative cumulative frequency analysis in indirect calorimetry: application to studies of transgenic mice. *Canadian Journal of Physiology and Pharmacology* **82**,101 (2004).

257. Lam, J. *et al.* A Universal Approach to Analyzing Transmission Electron Microscopy with ImageJ. *Cells* **10**, 2177 (2021).

258. Guo, W., Jiang, L., Bhasin, S., Khan, S. M. & Swerdlow, R. H. DNA extraction procedures meaningfully influence qPCR-based mtDNA copy number determination. *Mitochondrion* **9**, 261–265 (2009).

259. Aarsland, A., Chinkes, D. & Wolfe, R. R. Hepatic and whole-body fat synthesis in humans during carbohydrate overfeeding. *The American Journal of Clinical Nutrition* **65**, 1774–1782 (1997).

260. Minehira, K., Vega, N., Vidal, H., Acheson, K. & Tappy, L. Effect of carbohydrate overfeeding on whole body macronutrient metabolism and expression of lipogenic enzymes in adipose tissue of lean and overweight humans. *International Journal of Obesity* **28**, 1291–1298 (2004).

261. Fausnacht, D. W. *et al.* Heat Stress Reduces Metabolic Rate While Increasing Respiratory Exchange Ratio in Growing Pigs. *Animals* **11**, 215 (2021).

262. Kalinovich, A. V., Jong, J. M. A. de, Cannon, B. & Nedergaard, J. UCP1 in adipose tissues: two steps to full browning. *Biochimie* **134**, 127–137 (2017).

263. Himms-Hagen, J. Brown adipose tissue thermogenesis: interdisciplinary studies. *The FASEB Journal* **4**, 2890–2898 (1990).

264. Arbuthnott, E. Brown adipose tissue: structure and function. *The Proceedings of the Nutrition Society* **48**, 177–82 (1989).

265. Nedergaard, J. *et al.* UCP1: the only protein able to mediate adaptive non-shivering thermogenesis and metabolic inefficiency. *Biochimica et Biophysica Acta (BBA) - Bioenergetics* **1504**, 82–106 (2001).

266. Binzen, C. A., Swan, P. D. & Manore, M. M. Postexercise oxygen consumption and substrate use after resistance exercise in women: *Medicine and Science in Sports and Exercise* **33**, 932–938 (2001).

267. Haddock, B. L. & Wilkin, L. D. Resistance Training Volume and Post Exercise Energy Expenditure. *Int J Sports Med* **27**, 143–148 (2006).

268. Melby, C., Scholl, C., Edwards, G. & Bullough, R. Effect of acute resistance exercise on postexercise energy expenditure and resting metabolic rate. *Journal of Applied Physiology* **75**, 1847–1853 (1993).

269. Ormsbee, M. J. *et al.* Fat metabolism and acute resistance exercise in trained men. *Journal of Applied Physiology* **102**, 1767–1772 (2007).

270. Yoo, H. S. *et al.* Intermittent Cold Exposure Enhances Fat Accumulation in Mice. *PLoS ONE* **9**, e96432 (2014).

271. Fischer, A. W., Csikasz, R. I., Von Essen, G., Cannon, B. & Nedergaard, J. No insulating effect of obesity. *American Journal of Physiology-Endocrinology and Metabolism* **311**, E202–E213 (2016).

272. Som, R., Fink, B. D., Yu, L. & Sivitz, W. I. Oxaloacetate regulates complex II respiration in brown fat: dependence on UCP1 expression. *American Journal of Physiology-Cell Physiology* 102-120 (2023) doi:10.1152/ajpcell.00565.2022.

273. Cameron, I. L. & Smith, R. E. Cytological responses of brown fat tissue in cold-exposed rats. *The Journal of Cell Biology* **23**, 89–100 (1964).

274. Yamashita, H. *et al.* Basic fibroblast growth factor (bFGF) contributes to the enlargement of brown adipose tissue during cold acclimation. *Pflügers Archiv European Journal of Physiology* **428**, 112-121(1994).

275. Park, I. R. & Himms-Hagen, J. Neural influences on trophic changes in brown adipose tissue during cold acclimation. *The American journal of physiology* **255**, R874-81 (1988).

276. Hare, J. F. & Hodges, R. Turnover of mitochondrial inner membrane proteins in hepatoma monolayer cultures. *Journal of Biological Chemistry* **257**, 3575–3580 (1982).

277. Moazed, B. & Desautels, M. Differentiation-dependent expression of cathepsin D and importance of lysosomal proteolysis in the degradation of UCP1 in brown adipocytes. *Canadian Journal of Physiology and Pharmacology* **80**, 515–525 (2002).

278. Eskelinen, E.-L. To be or not to be? Examples of incorrect identification of autophagic compartments in conventional transmission electron microscopy of mammalian cells. *Autophagy* **4**, 257–260 (2008).

279. Watanabe, J., Kanamura, S., Tokunaga, H., Sakaida, M. & Kanai, K. Significance of increase in glucose 6-phosphatase activity in brown adipose cells of cold-exposed and starved mice. *The Anatomical Record* **219**, 39–44 (1987).

280. Williams, J. A. & Ding, W.-X. Mechanisms, pathophysiological roles and methods for analyzing mitophagy – recent insights. *Biological Chemistry* **399**, 147–178 (2018).

281. Chen, M. *et al.* Mitophagy receptor FUNDC1 regulates mitochondrial dynamics and mitophagy. *Autophagy* **12**, 689–702 (2016).

282. Wani, W. Y. *et al.* Regulation of autophagy by protein post-translational modification. *Laboratory Investigation* **95**, 14–25 (2015).

283. Lass, A. *et al.* Adipose triglyceride lipase-mediated lipolysis of cellular fat stores is activated by CGI-58 and defective in Chanarin-Dorfman Syndrome. *Cell Metabolism* **3**, 309–319 (2006).

284. Schreiber, R. *et al.* Cold-Induced Thermogenesis Depends on ATGL-Mediated Lipolysis in Cardiac Muscle, but Not Brown Adipose Tissue. *Cell Metabolism* **26**, 753-763.e7 (2017).

285. Shin, H. *et al.* Lipolysis in Brown Adipocytes Is Not Essential for Cold-Induced Thermogenesis in Mice. *Cell Metabolism* **26**, 764-777.e5 (2017).

286. Zechner, R. *et al.* FAT SIGNALS - Lipases and Lipolysis in Lipid Metabolism and Signaling. *Cell Metabolism* **15**, 279–291 (2012).

287. Huang, Y. *et al.* Heat stress promotes lipid accumulation by inhibiting the AMPK-PGC-1α signaling pathway in 3T3-L1 preadipocytes. *Cell Stress and Chaperones* **26**, 563–574 (2021).

288. Hori, K. *et al.* Memory of long-term cold acclimation in deacclimated Wistar rats. *Journal of Thermal Biology* **31**, 124–130 (2006).

289. Montava-Garriga, L., Singh, F., Ball, G. & Ganley, I. G. Semi-automated quantitation of mitophagy in cells and tissues. *Mechanisms of Ageing and Development* **185**, 111-196 (2020).

290. Smaal, E. B., Romijn, D., Geurts Van Kessel, W. S., De Kruijff, B. & De Gier, J. Isolation and purification of cardiolipin from beef heart. *Journal of Lipid Research* **26**, 634–637 (1985).

291. Daum, G. & Vance, J. E. Import of lipids into mitochondria. *Progress in Lipid Research* **36**, 103–130 (1997).

292. Schlame, M. Thematic Review Series: Glycerolipids. Cardiolipin synthesis for the assembly of bacterial and mitochondrial membranes. *Journal of Lipid Research* **49**, 1607–1620 (2008).

293. Houtkooper, R. H. & Vaz, F. M. Cardiolipin, the heart of mitochondrial metabolism. *Cell. Mol. Life Sci.* **65**, 2493–2506 (2008).

294. Paradies, G., Paradies, V., De Benedictis, V., Ruggiero, F. M. & Petrosillo, G. Functional role of cardiolipin in mitochondrial bioenergetics. *Biochimica et Biophysica Acta (BBA) - Bioenergetics* **1837**, 408–417 (2014).

295. Schrepfer, E. & Scorrano, L. Mitofusins, from Mitochondria to Metabolism. *Molecular Cell* **61**, 683–694 (2016).

296. Bustillo-Zabalbeitia, I. *et al.* Specific Interaction with Cardiolipin Triggers Functional Activation of Dynamin-Related Protein 1. *PLoS ONE* **9**, e102738 (2014).

297. Stepanyants, N. *et al.* Cardiolipin's propensity for phase transition and its reorganization by dynamin-related protein 1 form a basis for mitochondrial membrane fission. *MBoC* **26**, 3104–3116 (2015).

298. Bayir, H. *et al.* Selective early cardiolipin peroxidation after traumatic brain injury: an oxidative lipidomics analysis. *Annals of Neurology* **62**, 154–169 (2007).

299. Kagan, V. E. *et al.* Cytochrome c acts as a cardiolipin oxygenase required for release of proapoptotic factors. *Nat Chem Biol* **1**, 223–232 (2005).

300. Kagan, V. E., Chu, C. T., Tyurina, Y. Y., Cheikhi, A. & Bayir, H. Cardiolipin asymmetry, oxidation and signaling. *Chemistry and Physics of Lipids* **179**, 64–69 (2014).

301. Garcia Fernandez, M. *et al.* Early changes in intramitochondrial cardiolipin distribution during apoptosis. *Cell Growth Differ* **13**, 449–455 (2002).

302. Kuwana, T. *et al.* Bid, Bax, and Lipids Cooperate to Form Supramolecular Openings in the Outer Mitochondrial Membrane. *Cell* **111**, 331–342 (2002).

303. Li, P. *et al.* Cytochrome c and dATP-Dependent Formation of Apaf-1/Caspase-9 Complex Initiates an Apoptotic Protease Cascade. *Cell* **91**, 479–489 (1997).

304. Zinser, E. *et al.* Phospholipid synthesis and lipid composition of subcellular membranes in the unicellular eukaryote Saccharomyces cerevisiae. *J Bacteriol* **173**, 2026–2034 (1991).

305. Gebert, N. *et al.* Mitochondrial Cardiolipin Involved in Outer-Membrane Protein Biogenesis: Implications for Barth Syndrome. *Current Biology* **19**, 2133–2139 (2009).

306. Chu, C. T. *et al.* Cardiolipin externalization to the outer mitochondrial membrane acts as an elimination signal for mitophagy in neuronal cells. *Nat Cell Biol* **15**, 1197–1205 (2013).

307. Youle, R. J. & Van Der Bliek, A. M. Mitochondrial Fission, Fusion, and Stress. *Science* **337**, 1062–1065 (2012).

308. Lutter, M. *et al.* Cardiolipin provides specificity for targeting of tBid to mitochondria. *Nat Cell Biol* **2**, 754–756 (2000).

309. Gonzalvez, F. *et al.* Cardiolipin provides an essential activating platform for caspase-8 on mitochondria. *The Journal of Cell Biology* **183**, 681–696 (2008).

310. Antón, Z. *et al.* Human Atg8-cardiolipin interactions in mitophagy: Specific properties of LC3B, GABARAPL2 and GABARAP. *Autophagy* **12**, 2386–2403 (2016).

311. Huang, W. *et al.* Crystal structure and biochemical analyses reveal Beclin 1 as a novel membrane binding protein. *Cell Res* **22**, 473–489 (2012).

312. Sustarsic, E. G. *et al.* Cardiolipin Synthesis in Brown and Beige Fat Mitochondria Is Essential for Systemic Energy Homeostasis. *Cell Metab* **28**, 159-174.e11 (2018).

313. Ogawa, K., Ohno, T. & Kuroshima, A. Muscle and brown adipose tissue fatty acid profiles in cold-exposed rats. *Jpn.J.Physiol* **37**, 783–796 (1987).

314. Ricquier, D., Mory, G., Nechad, M. & Hémon, P. Effects of cold adaptation and re-adaptation upon the mitochondrial phospholipids of brown adipose tissue. *J Physiol (Paris)* **74**, 695–702 (1978).

6. Contributions

All experiments were conducted by Nidhi Kuksal. Experiments were designed by Mary Ellen Harper, Chantal Pileggi, and Nidhi Kuksal. The data were analyzed by Nidhi Kuksal, Valeria Vasilyeva, Ziyad El Hankouri, and Ella McIlroy. The project was supervised by Mary-Ellen Harper. Funding for the research was acquired by Mary-Ellen Harper from the Natural Sciences and Engineering Research Council (NSERC) of Canada.